

Baryon and lepton numbers in particle physics beyond the standard model

Thesis by

Jonathan M. Arnold

In Partial Fulfillment of the Requirements

for the Degree of

Doctor of Philosophy



California Institute of Technology

Pasadena, California

2014

(Submitted May 2, 2014)

© 2014

Jonathan M. Arnold

All Rights Reserved

To my proud and loving parents, for their endless support

Abstract

The works presented in this thesis explore a variety of extensions of the standard model of particle physics which are motivated by baryon number (B) and lepton number (L), or some combination thereof. In the standard model, both baryon number and lepton number are accidental global symmetries violated only by non-perturbative weak effects, though the combination $B - L$ is exactly conserved. Although there is currently no evidence for considering these symmetries as fundamental, there are strong phenomenological bounds restricting the existence of new physics violating B or L . In particular, there are strict limits on the lifetime of the proton whose decay would violate baryon number by one unit and lepton number by an odd number of units.

The first paper in this thesis explores some of the simplest possible extensions of the standard model in which baryon number is violated, but the proton does not decay as a result. The second paper extends this analysis to explore models in which baryon number is conserved, but lepton flavor violation is present. Special attention is given to the processes of μ to e conversion and $\mu \rightarrow e\gamma$ which are bound by existing experimental limits and relevant to future experiments.

The final two papers explore extensions of the minimal supersymmetric standard model (MSSM) in which both baryon number and lepton number, or the combination $B - L$, are elevated to the status of being spontaneously broken local symmetries. These models have a rich phenomenology including new collider signatures, stable dark matter candidates, and alternatives to the discrete R-parity symmetry usually built into the MSSM in order to protect against baryon and lepton number violating processes.

Contents

Acknowledgments	iv
Abstract	v
1 Introduction	1
2 Simplified models with baryon number violation but no proton decay	6
2.1 Introduction	6
2.2 The models	8
2.3 Phenomenology of model 1	15
2.3.1 Neutron-antineutron oscillations	15
2.3.2 LHC, flavor and electric dipole moment constraints	18
2.3.3 Baryon asymmetry	20
2.4 Conclusions	22
Appendices	24
2.A Vacuum insertion approximation	24
2.B Down quark edm	25
2.C K^0 - \bar{K}^0 mixing	28
2.D Absorptive part of X_2 decay	29
3 Phenomenology of scalar leptoquarks	32
3.1 Introduction	32

3.2	Models	33
3.3	Phenomenology	35
3.3.1	Naturalness	35
3.3.2	$\mu \rightarrow e\gamma$ decay	36
3.3.3	$\mu \rightarrow e$ conversion	38
3.3.4	Electron EDM	43
3.4	Baryon number violation and dimension five operators	45
3.5	Conclusions	47
Appendices		49
3.A	Calculation of $\mu \rightarrow e\gamma$	49
4	Supersymmetric Dark Matter Sectors	53
4.1	Introduction	53
4.2	Supersymmetric Dark Sector	55
4.3	Dark Matter Relic Density	59
4.4	Predictions for DM Direct Detection	62
4.5	Conclusions	65
5	B and L at the SUSY Scale, Dark Matter and R-parity Violation	67
5.1	Introduction	67
5.2	Spontaneous Breaking of B and L	69
5.2.1	Symmetry Breaking and Gauge Boson Masses	71
5.2.2	Spontaneous R-parity Violation	74
5.3	Dark Matter Candidates	75
5.4	Conclusions	79
Bibliography		81

Chapter 1

Introduction

This thesis details some of the research I have completed during my time as a graduate student at Caltech. My focus has been on building models of particle physics for physics beyond the standard model. The works presented here explore a variety of models which give special attention to the symmetries associated with baryon number and lepton number – accidental global symmetries in the standard model which are violated only non-perturbatively via the weak interactions. In Chapters 2 and 3, we explore the minimal models which violate these symmetries without being in conflict with existing experimental bounds, especially bounds on proton decay. The models proposed in these chapters can be described as simplified models. That is, rather than being led by a larger theoretical motivation such as grand unification or the hierarchy problem, we build models with a minimal number of new particles and interactions. Though it is not necessary, one can think of a simplified model as being the low energy limit of more complex new physics scenarios. In Chapters 4 and 5, we instead focus on extending the minimal supersymmetric standard model to include baryon and lepton numbers as more fundamental symmetries of nature. In these chapters, we take the hierarchy problem as motivation for the inclusion of supersymmetry, and we explore the possibility that baryon number (B) and lepton number (L), or the combination $B - L$, are spontaneously broken gauge symmetries. The resulting models have rich phenomenological consequences as well as attractive theoretical features.

As stated above, both baryon number and lepton number are accidental symmetries of

the standard model, and both are observed to be extremely good symmetries of nature. The proton, for example, is known to have a lifetime of at least $\sim 10^{34}$ years. However, there is no fundamental symmetry guaranteeing its absolute stability in the same way that, for example, electromagnetic gauge invariance guarantees the stability of the electron. In fact, it is known that both baryon and lepton numbers are violated by non-perturbative weak processes. This is due to the fact that, in the standard model, each of these global symmetries is anomalous. That is, they are classical symmetries of the standard model, but each is broken by non-perturbative quantum effects. Although these effects are small enough to be negligible in laboratory experiments, they can be important in studying the early universe when temperatures were much higher. Indeed, the standard modern cosmological models rely on a violation of baryon number to explain the matter asymmetry observed in the universe – a violation of B is one of the three Sakharov conditions necessary for baryogenesis. A violation of lepton number is another popular ingredient in early universe cosmology since a lepton asymmetry can generate a baryon asymmetry via B - and L -violating sphalerons – a mechanism known as leptogenesis. In any case, there is a tension between the apparent necessity for baryon and lepton number violation in models of early universe cosmology and the strict bounds placed on the violation of these symmetries generated by laboratory experiments. It is this tension, in part, which has motivated the works included in this thesis.

The first two chapters in this thesis were motivated by the first half of this tension. Chapter 2 explores the simplest possible models in which the classical conservation of baryon number in the standard model is violated by the addition of a minimal number of additional scalar degrees of freedom. Motivated by the extremely long lifetime of the proton, we focus on models in which the new sources of baryon number violation do not lead to proton decay at tree-level. We find and enumerate a set of nine models which satisfy this requirement with the addition of only two new scalar fields. Each model has a unique phenomenology, though neutral meson mixing, neutron-antineutron oscillation, and other baryon number violating processes are common among them. The models are

strongly constrained by both flavor physics and limits on the electric dipole moment of the neutron. We explore the parameter space of one model in particular to show that it can be in agreement with current experimental bounds, but still have measurable effects in the next generation of neutron oscillation experiments.

In Chapter 3, we use a very similar approach to model building, this time with the goal of exploring simple extensions of the standard model which include lepton flavor violation. In this case, models with (perturbative) baryon number violation in the Yukawa sector are ignored, and only models with a single additional scalar field are considered. Only two such models exist, one of which is characterized by an unusual enhancement to the lepton flavor violating process $\mu \rightarrow e\gamma$ proportional to the top quark mass. The phenomenology of this model is investigated in detail, including a careful calculation of the $\mu \rightarrow e\gamma$ decay rate, the $\mu \rightarrow e$ conversion rate, and the constraints coming from the electric dipole moment of the electron. We find that the model could have measurable effects in the charged lepton sector which would be observed at the MEG experiment ($\mu \rightarrow e\gamma$) and at the prospective Mu2e experiment ($\mu \rightarrow e$).

The last two chapters of this thesis were motivated by the second half of the tension mentioned earlier – the strict limits on the structure of new physics coming from measured bounds on baryon and lepton number violating processes in laboratory experiments. These works focus on the possibility that these symmetries are not simply accidental global symmetries of the low energy theory, but rather relics of some more fundamental spontaneously broken symmetry related to these numbers. In addition, the models are built into the minimal supersymmetric standard model (MSSM) in part because of the new gauge symmetries’ ability to replace R-parity, usually included in the MSSM to avoid dangerous B - and L -violating terms in the superpotential.

Chapter 4 develops an extension of the MSSM which includes a spontaneously broken $B - L$ symmetry. In the standard model and in the MSSM, $B - L$ is not anomalous if right-handed neutrinos are included, and so there is no additional particle content necessary to avoid the usual problems associated with anomalies in gauge theories. One advantage of

introducing $B - L$ as a spontaneously broken gauge symmetry is that it eliminates the need for an ad-hoc R-parity, usually introduced to explain away the existence of baryon and lepton number violating terms in the MSSM superpotential. In the model we introduce in Chapter 4, the MSSM is endowed with an extended gauge sector including $U(1)_{B-L}$. The gauge symmetry is broken by the vacuum expectation value of the right-handed sneutrino, which then communicates this breaking via the D-term to a dark sector charged under $B-L$. This process breaks supersymmetry in the dark sector and introduces a mass splitting among the new fields. The lightest of these particles is a good dark matter candidate. One interesting feature of this model is that, although R-parity is broken in the visible sector, no discrete symmetry is needed to guarantee the stability of the dark matter candidate. We show that the dark matter in this model is capable of reproducing the measured thermal relic abundance while still escaping the experimental bounds set by Xenon100.

In Chapter 5, we take a similar approach to extending the MSSM, this time by introducing an extended gauge sector including $U(1)_B \otimes U(1)_L$. This gauge group has the advantage of eliminating non-renormalizable terms in the superpotential like $\hat{Q}\hat{Q}\hat{Q}\hat{L}/\Lambda$ and $\hat{u}^c\hat{u}^c\hat{d}^c\hat{e}^c/\Lambda$. These terms, which appear for example in $SU(5)$ extensions of the MSSM, do not violate either R-parity or $B - L$. However, bounds on proton decay limit the scale Λ to be greater than 10^{27} GeV – an enormous suppression that warrants theoretical grounding. Because these terms violate B and L separately, gauging these symmetries provides a simple possible mechanism for explaining this suppression. However, in the MSSM, $U(1)_B$ and $U(1)_L$ are anomalous symmetries and so cannot be gauged without introducing new particle content to cancel anomalies in this new gauge sector. In this chapter, we introduce a set of superfields we call leptoquarks with both B and L quantum numbers that do just that, as well as the minimal new field content necessary to spontaneously break these local symmetries. We find that the breaking scale of $U(1)_B \otimes U(1)_L$ and supersymmetry are related, so the B and L breaking scale must be relatively low if we expect supersymmetry to provide a solution to the hierarchy problem. In addition, the model has a remnant Z_2 which protects the lightest of these leptoquarks from decay. Thus the lightest of these new

particles represents a possible dark matter candidate whose phenomenology we explore.

This collection of work studies a variety of extensions of the standard model motivated by the apparent importance of baryon number violation (and possibly lepton number violation) in the early universe and the apparent lack of baryon and lepton number violation measured in experiment. Future experiments testing baryon number violation via proton decay and neutron oscillation, lepton number violation via double beta decay, and lepton flavor violation via $\mu \rightarrow e\gamma$ and $\mu \rightarrow e$ conversion will help constrain or reveal new physics related to these symmetries. Meanwhile, new cosmological measurements may help guide theory to the correct model of baryogenesis to explain the matter asymmetry in the universe.

Chapter 2

Simplified models with baryon number violation but no proton decay

2.1 Introduction

The standard model has non-perturbative violation of baryon number (B). This source of baryon number non-conservation also violates lepton number (L), however, it conserves baryon number minus lepton number ($B - L$). The violation of baryon number by non-perturbative weak interactions is important at high temperatures in the early universe, but it has negligible impact on laboratory experiments that search for baryon number violation and we neglect it in this paper. If we add massive right-handed neutrinos that have a Majorana mass term and Yukawa couple to the standard model left-handed neutrinos, then lepton number is violated by two units, $|\Delta L| = 2$, at tree-level in the standard model.

Motivated by Grand Unified Theories (GUT) there has been an ongoing search for proton decay (and bound neutron decay). The limits on possible decay modes are very strong. For example, the lower limit on the partial mean lifetime for the mode $p \rightarrow e^+ \pi^0$ is 8.2×10^{33} yrs [46]. All proton decays violate baryon number by one unit and lepton number by an odd number of units. See Ref. [71] for a review of proton decay in extensions of the standard model.

There are models where baryon number is violated, but proton (and bound neutron) decay does not occur. This paper is devoted to finding the simplest models of this type

and discussing some of their phenomenology. We include all renormalizable interactions allowed by the $SU(3) \times SU(2) \times U(1)$ gauge symmetry. In addition to standard model fields these models have scalar fields $X_{1,2}$ that couple to quark bilinear terms or lepton bilinear terms. Baryon number violation either occurs through trilinear scalar interactions of the type (i) $X_2 X_1 X_1$ or quartic scalar terms of the type (ii) $X_2 X_1 X_1 X_1$. The cubic scalar interaction in (i) is similar in structure to renormalizable terms in the superpotential that give rise to baryon number violation in supersymmetric extensions of the standard model. However, in our case the operator is dimension three and is in the scalar potential. Assuming no right-handed neutrinos there are four models of type (i) where each of the X 's couples to quark bilinears and has baryon number $-2/3$. Hence in this case the X 's are either color $\mathbf{3}$ or $\bar{\mathbf{6}}$. There are also five models of type (ii) where X_1 is a color $\mathbf{3}$ or $\bar{\mathbf{6}}$ with baryon number $-2/3$ that couples to quark bilinears and X_2 is a color singlet with lepton number -2 that couples to lepton bilinears.

We analyze one of the models in more detail. In that model the $SU(3) \times SU(2) \times U(1)$ quantum numbers of the new colored scalars are $X_1 = (\bar{\mathbf{6}}, 1, -1/3)$ and $X_2 = (\bar{\mathbf{6}}, 1, 2/3)$. The $n\bar{n}$ oscillation frequency is calculated using the vacuum insertion approximation for the required hadronic matrix element and lattice QCD results. For dimensionless coupling constants equal to unity and all mass parameters equal, the present absence of observed $\bar{n}n$ oscillations provides a lower limit on the scalar masses of around 500 TeV. If we consider the limit $M_1 \ll M_2$ then for $M_1 = 5$ TeV the next generation of $n\bar{n}$ oscillation experiments will be sensitive to M_2 masses at the GUT scale.

There are three models that have $n\bar{n}$ mixing at tree-level without proton decay. In these models, constraints on flavor changing neutral currents and the electric dipole moment (edm) of the neutron require some very small dimensionless couplings constants if we are to have both observable $n\bar{n}$ oscillations and one of the scalar masses approaching the GUT scale.

In the next section we enumerate the models and discuss their basic features. The phenomenology of one of the models is discussed in more detail in Section 2.3. Some

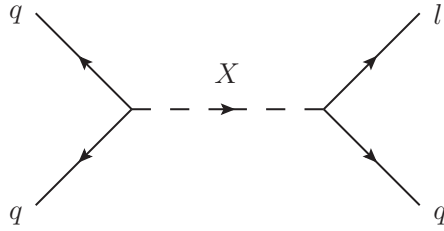


Figure 2.1: $\Delta B = 1$ and $\Delta L = 1$ scalar exchange.

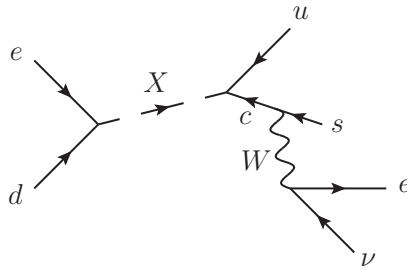


Figure 2.2: Feynman diagram that contributes to tree-level $p \rightarrow K^+ e^+ e^- \bar{\nu}$ from $(3, 1, -4/3)$ scalar exchange.

concluding remarks are given in Section 2.4.

2.2 The models

We are looking for the simplest models which violate baryon number, but don't induce proton decay. We don't impose any global symmetries. Hence, all local renormalizable interactions permitted by Lorentz and gauge invariance are assumed to be present. We begin by considering renormalizable scalar couplings with all possible standard model fermion bilinears. A similar philosophy can be used to construct models involving proton decay [3] or baryon number violating interactions in general [4, 5]. We first eliminate any scalars which produce proton decay via tree-level scalar exchange as in Fig. 2.1. In particular, this eliminates the scalars with $SU(3) \times SU(2) \times U(1)$ quantum numbers $(3, 1, -1/3)$, $(3, 3, -1/3)$, and $(3, 1, -4/3)$. Note that in the case of $(3, 1, -4/3)$ we need an additional W -boson ex-

change to get proton decay (Fig. 2.2) since the Yukawa coupling to right-handed charge $2/3$ quarks is antisymmetric (for a detailed discussion see [6]). The remaining possible scalar representations and Yukawa couplings are listed in Table 2.1. We have assumed there are no right-handed neutrinos (ν_R) in the theory.

operator	$SU(3) \times SU(2) \times U(1)$ rep. of X	B	L
XQQ, Xud	$(\bar{6}, 1, -1/3), (3, 1, -1/3)_{\text{PD}}$	$-2/3$	0
XQQ	$(\bar{6}, 3, -1/3), (3, 3, -1/3)_{\text{PD}}$	$-2/3$	0
Xdd	$(3, 1, 2/3), (\bar{6}, 1, 2/3)$	$-2/3$	0
Xuu	$(\bar{6}, 1, -4/3), (3, 1, -4/3)_{\text{PD}}$	$-2/3$	0
XQL	$(3, 1, -1/3)_{\text{PD}}, (3, 3, -1/3)_{\text{PD}}$	$1/3$	1
$X\bar{u}\bar{e}$	$(3, 1, -1/3)_{\text{PD}}$	$1/3$	1
$Xd\bar{e}$	$(3, 1, -4/3)_{\text{PD}}$	$1/3$	1
$XQe, XL\bar{u}$	$(3, 2, 7/6)$	$1/3$	-1
XLd	$(\bar{3}, 2, -1/6)_{\text{PD}}$	$-1/3$	1
XLL	$(1, 1, 1), (1, 3, 1)$	0	-2
Xee	$(1, 1, 2)$	0	-2

Table 2.1: Possible interaction terms between the scalars and fermion bilinears along with the corresponding quantum numbers and B and L charges of the X field. Representations labeled with the subscript ‘‘PD’’ allow for proton decay via either tree-level scalar exchange (Fig. 2.1) or 3-scalar interactions involving the Higgs vev (Fig. 2.4).

None of these scalars induces baryon number violation on their own, so we consider minimal models with the requirement that only two unique sets of scalar quantum numbers from Table 2.1 are included, though a given set of quantum numbers may come with multiple scalars.

Baryon number violation will arise from terms in the scalar potential, so we need to take into account just the models whose scalar quantum numbers are compatible in the sense that they allow scalar interactions that violate baryon number. For scalars coupling to standard model fermion bilinears there are three types of scalar interactions which may violate baryon number: 3-scalar $X_1X_1X_2$, 4-scalar $X_1X_1X_1X_2$, and 3-scalar with a Higgs $X_1X_1X_1H$ or $X_1X_1X_2H$, where the Higgs gets a vacuum expectation value (vev) (Fig. 2.3).

Actually, the simplest possible model violating baryon number through the interaction

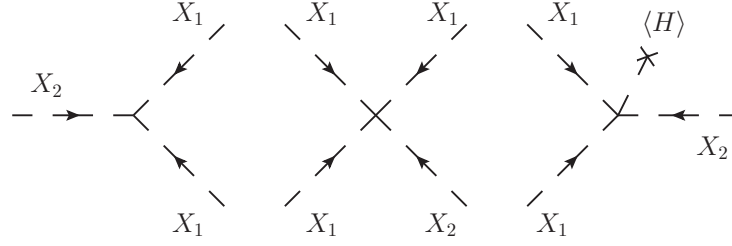


Figure 2.3: Scalar interactions which may generate baryon number violation.

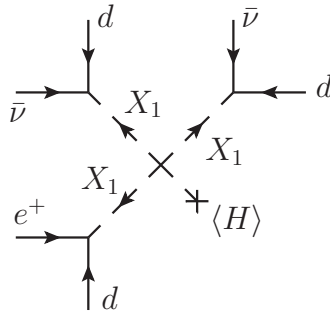


Figure 2.4: Interaction which leads to proton decay, $p \rightarrow \pi^+\pi^+e^-\nu\nu$, for $X_1 = (\bar{3}, 2, -1/6)$.

$X_1X_1X_1H$ includes just one new scalar $(\bar{3}, 2, -1/6)$, but it gives proton decay via $p \rightarrow \pi^+\pi^+e^-\nu\nu$ (Fig. 2.4). Note that a similar diagram with $\langle H \rangle$ replaced by X_2 allows us to ignore scalars with the same electroweak quantum numbers as the Higgs and coupling to $\bar{Q}u$ and $\bar{Q}d$, $X_2 = (1, 2, 1/2)$ and $(8, 2, 1/2)$, as these will produce tree level proton decay as well. The other two baryon number violating models with an interaction term $X_1X_1X_2H$ are: $X_1^* = (3, 1, -1/3)$, $X_2 = (\bar{3}, 2, -7/6)$ and $X_1 = (3, 1, -1/3)$, $X_2^* = (\bar{3}, 2, -1/6)$. As argued earlier, such quantum numbers for X_1 also induce tree-level proton decay, so we disregard them.

We now consider models with a 3-scalar interaction $X_1X_1X_2$. A straightforward analysis shows that there are only four models which generate baryon number violation via a 3-scalar interaction without proton decay. We enumerate them and give the corresponding Lagrangians below. All of these models give rise to processes with $\Delta B = 2$ and $\Delta L = 0$,

but only the first three models contribute to $n\bar{n}$ oscillations at tree-level due to the symmetry properties of the Yukawas. Note that a choice of normalization for the sextet given by,

$$(X^{\alpha\beta}) = \begin{pmatrix} \tilde{X}^{11} & \tilde{X}^{12}/\sqrt{2} & \tilde{X}^{13}/\sqrt{2} \\ \tilde{X}^{12}/\sqrt{2} & \tilde{X}^{22} & \tilde{X}^{23}/\sqrt{2} \\ \tilde{X}^{13}/\sqrt{2} & \tilde{X}^{23}/\sqrt{2} & \tilde{X}^{33} \end{pmatrix} \quad (2.1)$$

leads to canonically normalized kinetic terms for the elements $\tilde{X}^{\alpha\beta}$ and the usual form of the scalar propagator with symmetrized color indices. Unless otherwise stated, we will be using 2-component spinor notation. Parentheses indicate contraction of 2-component spinor indices to form a Lorentz singlet.

Model 1. $X_1 = (\bar{6}, 1, -1/3)$, $X_2 = (\bar{6}, 1, 2/3)$

$$\begin{aligned} \mathcal{L} = & -g_1^{ab} X_1^{\alpha\beta} (Q_{L\alpha}^a \epsilon Q_{L\beta}^b) - g_2^{ab} X_2^{\alpha\beta} (d_{R\alpha}^a d_{R\beta}^b) \\ & - g_1^{\prime ab} X_1^{\alpha\beta} (u_{R\alpha}^a d_{R\beta}^b) + \lambda X_1^{\alpha\alpha'} X_1^{\beta\beta'} X_2^{\gamma\gamma'} \epsilon_{\alpha\beta\gamma} \epsilon_{\alpha'\beta'\gamma'} \end{aligned} \quad (2.2)$$

By virtue of the symmetric color structure of the $\bar{6}$ representation and the antisymmetric weak structure of the QQ bilinear in the first term, g_1 must be antisymmetric in flavor. However, this antisymmetry is not retained upon rotation into the mass eigenstate basis. Similarly, g_2 must be symmetric because of the symmetric color structure in the second term. In this case, the symmetry character of g_2 will be retained upon rotation into the mass eigenstate basis because it involves quarks of the same charge. Therefore, the interaction involving the Yukawa coupling g_2 gives rise to (and is thus constrained by) K^0 - \bar{K}^0 mixing through tree-level X_2 exchange. The coupling g_1' has no particular flavor symmetry.

Model 2. $X_1 = (\bar{6}, 3, -1/3)$, $X_2 = (\bar{6}, 1, 2/3)$

$$\begin{aligned} \mathcal{L} = & -g_1^{ab} X_1^{\alpha\beta A} (Q_{L\alpha}^a \epsilon \tau^A Q_{L\beta}^b) - g_2^{ab} X_2^{\alpha\beta} (d_{R\alpha}^a d_{R\beta}^b) \\ & + \lambda X_1^{\alpha\alpha' A} X_1^{\beta\beta' A} X_2^{\gamma\gamma'} \epsilon_{\alpha\beta\gamma} \epsilon_{\alpha'\beta'\gamma'} \end{aligned} \quad (2.3)$$

Here the matrix $\epsilon \tau^A$ is symmetric. Because the first and second terms have symmetric color structures, g_1 and g_2 must be symmetric in flavor. The weak triplet X_1 has components which introduce both $K^0-\bar{K}^0$ and $D^0-\bar{D}^0$ mixing. As in model 1, the interaction involving g_2 will introduce $K^0-\bar{K}^0$ mixing via X_2 exchange.

Model 3. $X_1 = (\bar{6}, 1, 2/3)$, $X_2 = (\bar{6}, 1, -4/3)$

$$\begin{aligned} \mathcal{L} = & -g_1^{ab} X_1^{\alpha\beta} (d_{R\alpha}^a d_{R\beta}^b) - g_2^{ab} X_2^{\alpha\beta} (u_{R\alpha}^a u_{R\beta}^b) \\ & + \lambda X_1^{\alpha\alpha'} X_1^{\beta\beta'} X_2^{\gamma\gamma'} \epsilon_{\alpha\beta\gamma} \epsilon_{\alpha'\beta'\gamma'} \end{aligned} \quad (2.4)$$

Both terms have symmetric color structures and no weak structure, so g_1 and g_2 must be symmetric in flavor. In this model, the interactions involving g_1 and g_2 each have the potential to introduce neutral meson-antimeson mixing. For example, the g_1 interaction will induce $K^0-\bar{K}^0$ mixing while g_2 will induce $D^0-\bar{D}^0$ mixing.

Model 4. $X_1 = (3, 1, 2/3)$, $X_2 = (\bar{6}, 1, -4/3)$

$$\begin{aligned} \mathcal{L} = & -g_1^{ab} X_{1\alpha} (d_{R\beta}^a d_{R\gamma}^b) \epsilon^{\alpha\beta\gamma} - g_2^{ab} X_2^{\alpha\beta} (u_{R\alpha}^a u_{R\beta}^b) \\ & + \lambda X_{1\alpha} X_{1\beta} X_2^{\alpha\beta} \end{aligned} \quad (2.5)$$

Because of the antisymmetric color structure in the first term, g_1 must be antisymmetric in flavor which prevents it from introducing meson-antimeson mixing. The antisymmetric structure of g_1 also prevents the existence of six-quark operators involving all first-generation quarks, and thus prevents $n\bar{n}$ oscillations. As in previous models, g_2 is symmet-

ric and so we will get $D^0\text{-}\bar{D}^0$ mixing as in model 3. Although this model does not have $n\bar{n}$ oscillations, there are still baryon number violating processes which would constrain this model – for example, the process $pp \rightarrow K^+K^+$. This has been searched using the Super-Kamiokande detector looking for the nucleus decay $^{16}\text{O} \rightarrow ^{14}\text{C}K^+K^+$ [7]. Had we included ν_R , model 4 would have been excluded by tree-level scalar exchange.

Now, a similar line of reasoning applies to the case where we have a quartic scalar interaction term $X_1X_1X_1X_2$. The only models violating baryon number which don't generate proton decay (or bound neutron decay) are discussed briefly below. These last five models have dinucleon decay to leptons, but don't contribute to tree-level $n\bar{n}$ oscillations by virtue of their coupling to leptons.

Model 5. $X_1 = (\bar{6}, 1, -1/3)$, $X_2 = (1, 1, 1)$

$$\begin{aligned} \mathcal{L} = & -g_1^{ab} X_1^{\alpha\beta} (Q_{L\alpha}^a \epsilon Q_{L\beta}^b) - g_2^{ab} X_2 (L_L^a \epsilon L_L^b) \\ & - g_1'^{ab} X_1^{\alpha\beta} (u_{R\alpha}^a d_{R\beta}^b) \\ & + \lambda X_1^{\alpha\alpha'} X_1^{\beta\beta'} X_1^{\gamma\gamma'} X_2 \epsilon_{\alpha\beta\gamma} \epsilon_{\alpha'\beta'\gamma'} \end{aligned} \quad (2.6)$$

Similar arguments to those for the previous models tell us that g_1 and g_2 must be antisymmetric in flavor.

Model 6. $X_1 = (\bar{6}, 3, -1/3)$, $X_2 = (1, 1, 1)$

$$\begin{aligned} \mathcal{L} = & -g_1^{ab} X_1^{\alpha\beta A} (Q_{L\alpha}^a \epsilon \tau^A Q_{L\beta}^b) - g_2^{ab} X_2 (L_L^a \epsilon L_L^b) \\ & + \lambda X_1^{\alpha\alpha' A} X_1^{\beta\beta' B} X_1^{\gamma\gamma' C} X_2 \epsilon^{ABC} \epsilon_{\alpha\beta\gamma} \epsilon_{\alpha'\beta'\gamma'} \end{aligned} \quad (2.7)$$

By comparison with model 2, we see that g_1 is symmetric in flavor while g_2 is antisymmetric.

Model 7. $X_1 = (\bar{6}, 3, -1/3)$, $X_2 = (1, 3, 1)$

$$\begin{aligned} \mathcal{L} = & -g_1^{ab} X_1^{\alpha\beta A} (Q_{L\alpha}^a \epsilon \tau^A Q_{L\beta}^b) - g_2^{ab} X_2^A (L_L^a \epsilon \tau^A L_L^b) \\ & + \lambda X_1^{\alpha\alpha' A} X_1^{\beta\beta' B} X_1^{\gamma\gamma' C} X_2^D \epsilon_{\alpha\beta\gamma} \epsilon_{\alpha'\beta'\gamma'} \\ & \times (\delta^{AB} \delta^{CD} + \delta^{AC} \delta^{BD} + \delta^{AD} \delta^{BC}) \end{aligned} \quad (2.8)$$

Once again, as in model 2, we have a symmetric g_1 . The coupling g_2 must be symmetric in flavor as well.

Model 8. $X_1 = (\bar{6}, 1, 2/3)$, $X_2 = (1, 1, -2)$

$$\begin{aligned} \mathcal{L} = & -g_1^{ab} X_1^{\alpha\beta} (d_{R\alpha}^a d_{R\beta}^b) - g_2^{ab} X_2 (e_R^a e_R^b) \\ & + \lambda X_1^{\alpha\alpha'} X_1^{\beta\beta'} X_1^{\gamma\gamma'} X_2 \epsilon_{\alpha\beta\gamma} \epsilon_{\alpha'\beta'\gamma'} \end{aligned} \quad (2.9)$$

As in model 1, g_1 must be symmetric. The coupling g_2 must also be symmetric in flavor.

Model 9. $X_1 = (3, 1, 2/3)$, $X_2 = (1, 1, -2)$

$$\begin{aligned} \mathcal{L} = & -g_1^{ab} X_{1\alpha} (d_{R\beta}^a d_{R\gamma}^b) \epsilon^{\alpha\beta\gamma} - g_2^{ab} X_2 (e_R^a e_R^b) \\ & + \lambda X_{1\alpha} X_{1\beta} X_{1\gamma} X_2 \epsilon^{\alpha\beta\gamma} \end{aligned} \quad (2.10)$$

By comparison with model 4, we see that g_1 must be antisymmetric in flavor. The coupling g_2 is symmetric. Note that the antisymmetric color structure of the scalar interaction requires the existence of at least three different kinds of X_1 scalars for this coupling to exist. Including ν_R would eliminate model 9 for the same reason as model 4.

2.3 Phenomenology of model 1

In this section we present a detailed analysis of model 1. The corresponding calculations for the other models can be performed in a similar manner. Our work is partly motivated by the recently proposed $n\bar{n}$ oscillation experiment with increased sensitivity [8]. In addition to $n\bar{n}$ oscillations, we also analyze the cosmological baryon asymmetry generation in model 1 as well as flavor and electric dipole moment constraints. A brief comment on LHC phenomenology is made.

2.3.1 Neutron-antineutron oscillations

The topic of $n\bar{n}$ oscillations has been explored in the literature in various contexts. For some of the early works on the subject see [9, 10, 11, 12]. Recently, a preliminary study of the required hadronic matrix elements using lattice QCD has been carried out [13]. Reference [14] claims that a signal of $n\bar{n}$ oscillations has been observed.

The scalar content of model 1 we are considering is similar to the content of a unified model explored in [15]. The transition matrix element,

$$\Delta m = \langle \bar{n} | \mathcal{H}_{\text{eff}} | n \rangle, \quad (2.11)$$

leads to a transition probability for a neutron at rest to change into an antineutron after time t equal to $P_{n \rightarrow \bar{n}}(t) = \sin^2(|\Delta m| t)$.

Neglecting the coupling g_1 in the Lagrangian (2.2) (for simplicity) the effective $|\Delta B| = 2$ Hamiltonian that causes $n\bar{n}$ oscillations is,

$$\begin{aligned} \mathcal{H}_{\text{eff}} = & -\frac{(g_1^{11})^2 g_2^{11} \lambda}{4M_1^4 M_2^2} d_{Ri}^{\dot{\alpha}} d_{Ri'}^{\dot{\beta}} u_{Rj}^{\dot{\gamma}} d_{Rj'}^{\dot{\delta}} u_{Rk}^{\dot{\lambda}} d_{Rk'}^{\dot{\chi}} \epsilon_{\dot{\alpha}\dot{\beta}} \epsilon_{\dot{\gamma}\dot{\delta}} \epsilon_{\dot{\lambda}\dot{\chi}} \\ & \times \left(\epsilon_{ijk} \epsilon_{i'j'k'} + \epsilon_{i'jk} \epsilon_{ij'k'} + \epsilon_{ij'k} \epsilon_{i'jk'} + \epsilon_{ijk'} \epsilon_{i'j'k} \right) + \text{h.c.} \end{aligned} \quad (2.12)$$

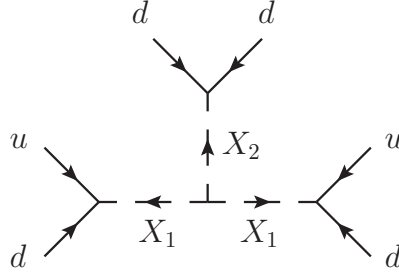


Figure 2.5: Interaction which leads to neutron-antineutron oscillations.

where Latin indices are color and Greek indices are spinor. It arises from the tree-level diagram in Fig. 2.5 (see, for example [16]). We have rotated the couplings g'_1 and g_2 to the quark mass eigenstate basis and adopted a phase convention where λ is real and positive. We estimate Δm using the vacuum insertion approximation [17]. This relates the required $n\bar{n}$ six quark matrix element to a matrix element from the neutron to the vacuum of a three quark operator. The later matrix element is relevant for proton decay and has been determined using lattice QCD methods. The general form of the required hadronic matrix elements is,

$$\langle 0 | d_{Ri}^{\dot{\alpha}} d_{Rj}^{\dot{\beta}} u_{Rk}^{\dot{\gamma}} | n(p, s) \rangle = -\frac{1}{18} \beta \epsilon_{ijk} \left(\epsilon^{\dot{\alpha}\dot{\gamma}} u_R^{\dot{\beta}}(p, s) + \epsilon^{\dot{\beta}\dot{\gamma}} u_R^{\dot{\alpha}}(p, s) \right). \quad (2.13)$$

Here u_R is the right-handed neutron two-component spinor and the Dirac equation was used to remove the term proportional to the left-handed neutron spinor. The constant β was determined using lattice methods in Ref. [18] to have the value $\beta \simeq 0.01 \text{ GeV}^3$. In the vacuum insertion approximation to Eq. (2.11) we find (see Appendix 2.A),

$$|\Delta m| = 2\lambda\beta^2 \frac{|(g_1^{11})^2 g_2^{11}|}{3M_1^4 M_2^2}. \quad (2.14)$$

We note that an analogous calculation using the MIT bag model was performed in Ref. [19]

and yields a similar result. The current experimental limit on Δm is [20],

$$|\Delta m| < 2 \times 10^{-33} \text{ GeV} . \quad (2.15)$$

For scalars of equal mass, $M_1 = M_2 \equiv M$, and the values of the couplings $g_1'^{11} = g_2'^{11} = 1$, $\lambda = M$, one obtains,

$$M \gtrsim 500 \text{ TeV} . \quad (2.16)$$

If, instead, the masses form a hierarchy, the effect on $n\bar{n}$ oscillations is maximized if we choose $M_2 > M_1$. Assuming $M_1 = 5 \text{ TeV}$ (above the current LHC reach) and $\lambda = M_2$ this yields,

$$M_2 \gtrsim 5 \times 10^{13} \text{ GeV} . \quad (2.17)$$

Note that $\lambda = M_2$ is a reasonable value for this coupling since integrating out M_2 then gives a quartic X_1 interaction term with a coupling on the order of one. Of course, this model does have a hierarchy problem so having the Higgs scalar and the X_1 light compared with X_2 requires fine tuning.

Experiments in the future [8] may be able to probe $n\bar{n}$ oscillations with increased sensitivity of $|\Delta m| \simeq 7 \times 10^{-35} \text{ GeV}$. If no oscillations are observed, the new limit in the case of equal masses will be,

$$M \gtrsim 1000 \text{ TeV} . \quad (2.18)$$

On the other hand, having $M_1 = 5 \text{ TeV}$ would push the mass of the heavier scalar up to the GUT scale, leading to the following constraint on the second scalar mass,

$$M_2 \gtrsim 1.5 \times 10^{15} \text{ GeV} . \quad (2.19)$$

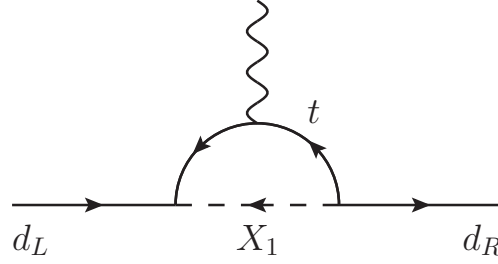


Figure 2.6: Diagram contributing to the electric dipole moment of the down quark.

We note, however, that in Section 2.3.2 we show that M_1 on the order of a few TeV is disfavored by the electric dipole moment constraints.

2.3.2 LHC, flavor and electric dipole moment constraints

If the mass of the scalar X_1 is small enough, it can be produced at the LHC through both single and pair production. Detailed analyses have been performed setting limits on the mass of X_1 from such processes [21, 22, 23]. A recent simulation [21] shows that 100 fb^{-1} of data from the LHC running at 14 TeV center of mass energy can be used to rule out or claim a discovery of X_1 scalars with masses only up to approximately 1 TeV, even when the couplings to quarks are of order 1. Our earlier choice of $M_1 = 5 \text{ TeV}$ used to estimate the constraint on M_2 from $n\bar{n}$ oscillations lies well within the allowed mass region.

Some of the most stringent flavor constraints on new scalars come from neutral meson mixing and electric dipole moments. The fact that in model 1, X_1 couples directly to both left- and right-handed quarks means that at one loop the top quark mass can induce the chirality flip necessary to give a light quark edm, putting strong constraints on this model even when X_1 is at the 100 TeV scale. The diagram contributing to the edm of the down quark is given in Fig. 2.6. We find (see Appendix 2.B),

$$|d_d| \simeq \frac{m_t}{6\pi^2 M_1^2} \log\left(\frac{M_1^2}{m_t^2}\right) \left| \text{Im}[g_1^{31}(g_1^{\prime 31})^*] \right| e \text{ cm} . \quad (2.20)$$

Here we have neglected pieces not logarithmically enhanced. This will give the largest

contribution to the neutron edm because of the top quark mass factor. All Yukawa couplings in this section are in the mass eigenstate basis.

Using $SU(6)$ wavefunctions, this can be related to the neutron edm via $d_n = \frac{4}{3}d_d - \frac{1}{3}d_u \simeq \frac{4}{3}d_d$. The present experimental limit is [24],

$$d_n^{\text{exp}} < 2.9 \times 10^{-26} \text{ e cm} . \quad (2.21)$$

Assuming $M_1 = 500 \text{ TeV}$, neutron edm measurements imply the bound $|\text{Im}[g_1^{31}(g_1^{31})^*]| \lesssim 6 \times 10^{-3}$. Furthermore, for observable $n\bar{n}$ oscillation effects with M_2 being close to the GUT scale we need $M_1 \approx 5 \text{ TeV}$. In such a scenario the edm constraint requires $|\text{Im}[g_1^{31}(g_1^{31})^*]| \lesssim 10^{-6}$.

Another important constraint on the parameters of model 1 is provided by $K^0\text{-}\bar{K}^0$ mixing. Integrating out X_2 generates an effective Hamiltonian,

$$\begin{aligned} \mathcal{H}_{\text{eff}} &= \frac{g_2^{22} (g_2^{11})^*}{M_2^2} (s_{R\alpha} s_{R\beta}) (d_R^{*\alpha} d_R^{*\beta}) \\ &\rightarrow \frac{g_2^{22} (g_2^{11})^*}{2M_2^2} (\bar{d}_R^\alpha \gamma^\mu s_{R\alpha}) (\bar{d}_R^\beta \gamma_\mu s_{R\beta}), \end{aligned} \quad (2.22)$$

where in the second line we have gone from two- to four-component spinor notation (see Appendix 2.C). This gives the following constraints on the couplings [25],

$$|\text{Re}[g_2^{22} (g_2^{11})^*]| < 1.8 \times 10^{-6} \left(\frac{M_2}{1 \text{ TeV}} \right)^2, \quad (2.23)$$

$$|\text{Im}[g_2^{22} (g_2^{11})^*]| < 6.8 \times 10^{-9} \left(\frac{M_2}{1 \text{ TeV}} \right)^2. \quad (2.24)$$

If we set M_2 to 500 TeV, this corresponds to an upper bound on the real and imaginary parts of $g_2^{22} (g_2^{11})^*$ of 0.45 and 1.7×10^{-3} , respectively.

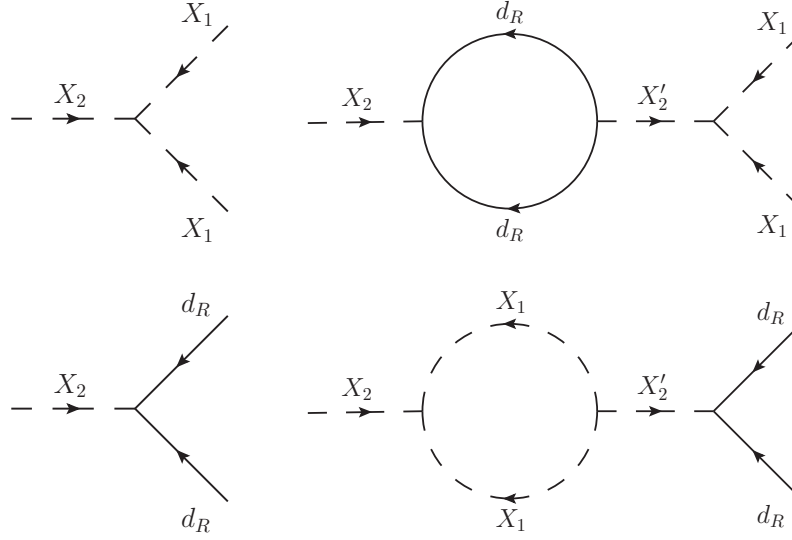


Figure 2.7: Diagrams corresponding to the decay of X_2 . The diagrams on top contribute to the $\Delta B = 2$ decays, while the diagrams on bottom contribute to $\Delta B = 0$.

Decay	Br	B_f
$X_2 \rightarrow \bar{X}_1 \bar{X}_1$	r	$4/3$
$X_2 \rightarrow \bar{d}_R \bar{d}_R$	$1 - r$	$-2/3$
$\bar{X}_2 \rightarrow X_1 X_1$	\bar{r}	$-4/3$
$\bar{X}_2 \rightarrow d_R d_R$	$1 - \bar{r}$	$2/3$

Table 2.2: Branching ratios and final state baryon numbers for the decays of X_2 and \bar{X}_2 which contribute to the baryon asymmetry in the coupling hierarchy $\lambda, \tilde{\lambda} \ll g_2, \tilde{g}_2$.

2.3.3 Baryon asymmetry

We now investigate baryon number generation in model 1. B and L violating processes in cosmology have been studied in the literature in great detail (for early works, see [26, 27]). We treat X_2 as much heavier than X_1 and use two different X_2 's to get a CP violating phase in the one-loop diagrams that generate the baryon asymmetry. For this calculation X_1 is treated as stable with baryon number $-2/3$ as each will eventually decay via baryon number conserving processes to two antiquarks. To simplify our discussion, let's consider the case in which the couplings satisfy the hierarchy $\lambda, \tilde{\lambda} \ll g_2, \tilde{g}_2$. The top line of Fig. 2.7 shows the dominant tree-level and one-loop diagrams contributing to the baryon number

violating decays of X_2 . Rotating the X fields to make the couplings λ and $\tilde{\lambda}$ real we find (see Appendix 2.D),

$$\begin{aligned}\Gamma(X_2 \rightarrow \bar{X}_1 \bar{X}_1) &= \frac{3\lambda}{8\pi M_2} \left[\lambda - \tilde{\lambda} \frac{M_2^2}{4\pi(M_2^2 - \tilde{M}_2^2)} \text{Im}(\text{Tr}(g_2^\dagger \tilde{g}_2)) \right], \\ \Gamma(\bar{X}_2 \rightarrow X_1 X_1) &= \frac{3\lambda}{8\pi M_2} \left[\lambda + \tilde{\lambda} \frac{M_2^2}{4\pi(M_2^2 - \tilde{M}_2^2)} \text{Im}(\text{Tr}(g_2^\dagger \tilde{g}_2)) \right].\end{aligned}\quad (2.25)$$

The net baryon number produced per $X_2 \bar{X}_2$ pair is (see, Table 2.2),

$$\begin{aligned}\Delta n_B &= 2(r - \bar{r}) \\ &= \frac{6}{\pi \text{Tr}(g_2^\dagger g_2)} \frac{1}{\tilde{M}_2^2 - M_2^2} \text{Im} \left[\lambda \tilde{\lambda}^* \text{Tr}(g_2^\dagger \tilde{g}_2) \right],\end{aligned}\quad (2.26)$$

where we have used the fact that CPT invariance guarantees the total width of X_2 and \bar{X}_2 are the same. Given our choice of hierarchy for the couplings, we have approximated the total width as coming from the tree-level decay of X_2 to antiquarks. A similar result in the context of $SO(10)$ models was obtained in Ref. [15].

Even with just one generation of quarks, the CP violating phase cannot be removed from the couplings λ , $\tilde{\lambda}$, g_2 , \tilde{g}_2 and a baryon asymmetry can be generated at one loop. At first glance this is surprising since there are four fields, X_2 , \bar{X}_2 , X_1 and d_R whose phases can be redefined and four relevant couplings. However, this can be understood by looking at the relevant Lagrangian terms, $g_2 X_2 d d$, $\tilde{g}_2 \bar{X}_2 d d$, $\lambda X_1 X_1 X_2$ and $\tilde{\lambda} X_1 X_1 \bar{X}_2$. The problem reduces to finding solutions to the following matrix equation,

$$\begin{pmatrix} 2 & 1 & 0 & 0 \\ 2 & 0 & 1 & 0 \\ 0 & 1 & 0 & 2 \\ 0 & 0 & 1 & 2 \end{pmatrix} \begin{pmatrix} \phi_{X_1} \\ \phi_{X_2} \\ \phi_{\bar{X}_2} \\ \phi_d \end{pmatrix} = \begin{pmatrix} \phi_\lambda \\ \phi_{\tilde{\lambda}} \\ \phi_{g_2} \\ \phi_{\tilde{g}_2} \end{pmatrix}, \quad (2.27)$$

where the phases on the right-hand side are arbitrary. Let us take the difference of the first two equations to remove phases for the couplings λ and $\tilde{\lambda}$, and the difference of the last

two equations to remove phases for the coupling g_2, \tilde{g}_2 . We therefore obtain $\phi_{\tilde{\lambda}_2} - \phi_{\lambda_2} = \phi_{\tilde{X}_2} - \phi_{X_2}$ and $\phi_{\tilde{g}_2} - \phi_{g_2} = \phi_{\tilde{X}_2} - \phi_{X_2}$. Those two equations cannot be simultaneously fulfilled for arbitrary $\phi_\lambda, \phi_{\tilde{\lambda}}, \phi_{g_2}, \phi_{\tilde{g}_2}$.

The baryon number generated in the early universe can be calculated from Eq. (2.26) by following the usual steps (see, for example, [28]). Out of equilibrium decay of X_2 and \tilde{X}_2 is most plausible if they are very heavy (e.g. $\sim 10^{12}$ GeV). However, to get measurable $n\bar{n}$ oscillation in this case, X_1 would have to be light – a case that is disfavored by neutron edm constraints, since it requires some very small dimensionless couplings.

2.4 Conclusions

We have investigated a set of minimal models which violate baryon number at tree-level without inducing proton decay. We have looked in detail at the phenomenological aspects of one of these models (model 1) which can have $n\bar{n}$ oscillations within the reach of future experiments. When all the mass parameters in model 1 have the same value, M , and the magnitudes of the Yukawa couplings g_1^{11} and g_2^{11} are unity, the present limit on $n\bar{n}$ oscillations implies that M is greater than 500 TeV. For $M = 500$ TeV, the neutron edm and flavor constraints give $\text{Im}[g_1^{31}(g_1^{31})^*] < 6 \times 10^{-6}$, $\text{Re}[g_2^{22}(g_2^{11})^*] < 0.45$, and $\text{Im}[g_2^{22}(g_2^{11})^*] < 1.7 \times 10^{-3}$ which indicates that some of the Yukawa couplings and/or their phases must be small if $n\bar{n}$ oscillations are to be observed in the next generation of experiments. Of course even in the standard model some of the Yukawa couplings are small.

There are two other models (model 2 and model 3) that have $n\bar{n}$ oscillations at tree-level. Similar conclusions can be drawn for them, although the details are different. In models 2 and 3, exchange of a single X_1 does not give rise to a one-loop edm of the neutron. However, K^0 - \bar{K}^0 mixing can occur from tree-level X_1 exchange.

Observable $n\bar{n}$ oscillations can occur for $M_2 \gg M_1$ with M_2 at/near the GUT scale.

This requires $M_1 \simeq 5$ TeV, and flavor and electric dipole constraints require some very small Yukawa couplings in that case.

Appendix

2.A Vacuum insertion approximation

We are trying to evaluate

$$\langle \bar{n}(p, s) | \mathcal{H}_{\text{eff}} | n(p, s) \rangle \quad (2.28)$$

where

$$\begin{aligned} \mathcal{H}_{\text{eff}} = & -\frac{(g_1^{11})^2 g_2^{11} \lambda}{4M_1^4 M_2^2} d_{Ri}^{\dot{\alpha}} d_{Ri'}^{\dot{\beta}} u_{Rj}^{\dot{\gamma}} d_{Rj'}^{\dot{\delta}} u_{Rk}^{\dot{\lambda}} d_{Rk'}^{\dot{\chi}} \epsilon_{\dot{\alpha}\dot{\beta}} \epsilon_{\dot{\gamma}\dot{\delta}} \epsilon_{\dot{\lambda}\dot{\chi}} \\ & \times \left(\epsilon_{ijk} \epsilon_{i'j'k'} + \epsilon_{i'jk} \epsilon_{ij'k'} + \epsilon_{ij'k} \epsilon_{i'jk'} + \epsilon_{ijk'} \epsilon_{i'j'k} \right) + \text{h.c.} \end{aligned} \quad (2.29)$$

using lattice results relevant to the matrix element

$$\langle 0 | d_{Ri}^{\dot{\alpha}} d_{Rj}^{\dot{\beta}} u_{Rk}^{\dot{\gamma}} | n(p, s) \rangle = -\frac{1}{18} \beta \epsilon_{ijk} \left(\epsilon^{\dot{\alpha}\dot{\gamma}} u_R^{\dot{\beta}}(p, s) + \epsilon^{\dot{\beta}\dot{\gamma}} u_R^{\dot{\alpha}}(p, s) \right). \quad (2.30)$$

The coefficient in front of the right-hand side of this equation is chosen to make connection with the lattice result in Ref. [18] which includes the contraction with $\epsilon^{ijk} \epsilon_{\dot{\alpha}\dot{\gamma}}$.

To estimate the matrix element Eq. (2.28), we look for rearrangements of the operator \mathcal{H}_{eff} which upon inserting the vacuum states $|0\rangle\langle 0|$ would give matrix elements of the form in Eq. (2.30). For example, \mathcal{H}_{eff} includes quark operators which can be rearranged as

$$d_{Ri}^{\dot{\alpha}} d_{Ri'}^{\dot{\beta}} u_{Rj}^{\dot{\gamma}} d_{Rj'}^{\dot{\delta}} u_{Rk}^{\dot{\lambda}} d_{Rk'}^{\dot{\chi}} = -d_{Ri}^{\dot{\alpha}} d_{Ri'}^{\dot{\beta}} u_{Rj}^{\dot{\gamma}} d_{Rj'}^{\dot{\delta}} d_{Rk'}^{\dot{\chi}} u_{Rk}^{\dot{\lambda}}. \quad (2.31)$$

Note that there are $\binom{4}{2}\binom{2}{1} = 12$ of these rearrangements possible. Inserting $|0\rangle\langle 0|$ into this choice gives a contribution

$$\begin{aligned} & -\langle \bar{n} | d_{Ri}^{\dot{\alpha}} d_{Ri'}^{\dot{\beta}} u_{Rj}^{\dot{\gamma}} | 0 \rangle \langle 0 | d_{Rj'}^{\dot{\delta}} d_{Rk'}^{\dot{\chi}} u_{Rk}^{\dot{\lambda}} | n \rangle \\ & = - \left(\frac{1}{18} \right)^2 |\beta|^2 \epsilon_{ii'j} \epsilon_{j'k'k} (\epsilon^{\dot{\alpha}\dot{\gamma}} v^{\dot{\beta}} + \epsilon^{\dot{\beta}\dot{\gamma}} v^{\dot{\alpha}}) (\epsilon^{\dot{\delta}\dot{\lambda}} u^{\dot{\chi}} + \epsilon^{\dot{\chi}\dot{\lambda}} u^{\dot{\delta}}). \end{aligned} \quad (2.32)$$

Finally, we contract this structure with the remaining color and weak epsilon tensors in Eq. (2.29) using the identities

$$\epsilon_{ijk} \epsilon_{ijk} = 6 \quad (2.33)$$

$$\epsilon_{imn} \epsilon_{jmn} = 2\delta_{ij} \quad (2.34)$$

$$\epsilon_{ijk} \epsilon_{imn} = 2\delta_{jm} \delta_{kn} - \delta_{jn} \delta_{km}. \quad (2.35)$$

It turns out this particular term contributes zero to the full matrix element because the color structure in \mathcal{H}_{eff} is symmetric under $(i \leftrightarrow i')$, $(j \leftrightarrow j')$, and $(k \leftrightarrow k')$. In fact, this reduces the number of non-zero contributions to just four of the twelve rearrangements. After evaluating these, we find the total contribution to be the result quoted in Eq. (2.14),

$$\langle \bar{n} | \mathcal{H}_{\text{eff}} | \rangle = |\Delta m| = 2\lambda\beta^2 \frac{|(g_1^{11})^2 g_2^{11}|}{3M_1^4 M_2^2}. \quad (2.36)$$

2.B Down quark edm

In computing the down-quark edm, we are looking for the coefficient of the operator

$$-\mathcal{L} = i \frac{d_d}{2} \bar{d}_L \sigma^{\mu\nu} F_{\mu\nu} d_R. \quad (2.37)$$

Starting with the Lagrangian

$$\mathcal{L} = -X_1^{\alpha\beta} [2g_1^{ab} (u_{L\alpha}^a d_{L\beta}^b) + g_1'^{ab} (u_{R\alpha}^a d_{R\beta}^b)] \quad (2.38)$$

we generate an effective Hamiltonian (integrating out X_1)

$$\begin{aligned}\mathcal{H}_{\text{eff}} &= -\frac{g_1^{ab}g_1'^{cd*}}{M_{X_1}^2}(u_{L\alpha}^a d_{L\beta}^b)(u_R^{c\alpha*} d_R^{d\beta*} + u_R^{c\beta*} d_R^{d\alpha*}) + \text{h.c.} \\ &\rightarrow -\frac{g_1^{13}g_1'^{31*}}{M_{X_1}^2}(t_{L\alpha} d_{L\beta})(t_R^{\alpha*} d_R^{\beta*} + t_R^{\beta*} d_R^{\alpha*}) + \text{h.c.}\end{aligned}\quad (2.39)$$

where in the second line we've focused on the top quark contribution which will dominate the dipole moment. Next, we write this using 4-component spinors by writing explicitly the spinor index contractions and then identifying the corresponding 4-component structure.

That is,

$$(t_{L\alpha} d_{L\beta}) = t_{L\alpha a} \epsilon^{ab} d_{L\beta b} = (t_\alpha^T C P_L d_\beta) \quad (2.40)$$

$$(t_{R\alpha} d_{R\beta}) = t_{L\alpha}^{\dot{a}} \epsilon_{\dot{a}\dot{b}} d_{L\beta}^{\dot{b}} = (t_\alpha^T C P_R d_\beta) . \quad (2.41)$$

Taking the hermitian conjugate of the second line gives

$$\begin{aligned}d^{\beta*T} (C P_R)^\dagger t^{\alpha*} &= \bar{d}^\beta \gamma^0 (C P_R)^\dagger \gamma^0 \bar{t}^{\alpha T} \\ &= \bar{d}^\beta \gamma^0 P_R^\dagger C^\dagger \gamma^0 \bar{t}^{\alpha T} \\ &= \bar{d}^\beta \gamma^0 P_R^\dagger \gamma^0 \gamma^0 C^\dagger \gamma^0 \bar{t}^{\alpha T} \\ &= \bar{d}^\beta P_L C \bar{t}^{\alpha T} \\ &= \bar{d}^\beta C P_L \bar{t}^{\alpha T}\end{aligned}\quad (2.42)$$

giving us an effective Hamiltonian in 4-component notation

$$\mathcal{H}_{\text{eff}} = -\frac{g_1^{ab}g_1'^{cd*}}{M_{X_1}^2}(t_\alpha^T C P_L d_\beta)(\bar{d}^\beta C P_L \bar{t}^{\alpha T} + \bar{d}^\alpha C P_L \bar{t}^{\beta T}) . \quad (2.43)$$

When evaluating the loop-diagram, we need to be careful with this effective Hamiltonian to make sure we get the correct sign associated the fermion loop in Fig. 2.6 generated once X_1 is integrated out as in Fig. 2.B.1. The time-ordered product associated with this

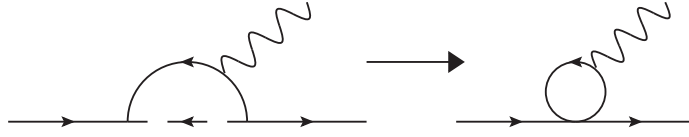


Figure 2.B.1: One-loop diagram contributing to the down quark edm.

diagram using just the first term in \mathcal{H}_{eff} is

$$\begin{aligned}
& \langle 0 | T \{ t_\alpha(x)_a (CP_L)_{ab} d_\beta(x)_b \bar{a} d_\beta(x)_c (CP_L)_{cd} \bar{t}_\alpha(x)_d \cdot \bar{t}_\alpha(y)_e \gamma_{ef}^\mu t_\alpha(y)_f \} | 0 \rangle \\
&= 3 S_{ae}^t(x-y) S_{fd}^t(y-x) \gamma_{ef}^\mu (CP_L)_{ab} (CP_L)_{cd} d_\beta(x)_b \bar{d}_\beta(x)_c \\
&= 3 (CP_L)_{ba}^T S_{ae}^t(x-y) \gamma_{ef}^\mu S_{fd}^t(y-x) (CP_L)_{dc}^T d_\beta(x)_b \bar{d}_\beta(x)_c
\end{aligned} \tag{2.44}$$

where we've left off the photon and defined

$$S_{ab}^t(x-y) = \langle 0 | T t_a(x) \bar{t}_b(y) | 0 \rangle . \tag{2.45}$$

Note that the second term in \mathcal{H}_{eff} contributes in the same way, but without the color factor of 3.

Next, we evaluate

$$4 \int \tilde{d}q (CP_L)^T \frac{i(\not{q} + m_t)}{q^2 - m_t^2} \gamma^\mu \frac{i(\not{q} + \not{k} + m_t)}{(q+k)^2 - m_t^2} (CP_L)^T \tag{2.46}$$

with q the incoming down quark momentum and k the outgoing photon momentum. The simplification of this is straightforward. Using

$$\gamma^\mu \gamma^\nu = \frac{1}{2} \{ \gamma^\mu, \gamma^\nu \} + \frac{1}{2} [\gamma^\mu, \gamma^\nu] = \frac{1}{2} \{ \gamma^\mu, \gamma^\nu \} - i \sigma^{\mu\nu} \tag{2.47}$$

we identify the piece coming from $\sigma^{\mu\nu}$

$$\begin{aligned}
& -4m_t P_L \int \tilde{d}q \frac{C \gamma^\mu \gamma^\nu k_\nu C}{[q^2 - m_t^2][(q+k)^2 - m_t^2]} \\
& \rightarrow 4im_t P_L C \sigma^{\mu\nu} k_\nu C \int \tilde{d}q \frac{1}{[q^2 - m_t^2][(q+k)^2 - m_t^2]} \\
& = \frac{4m_t P_L C \sigma^{\mu\nu} k_\nu C}{16\pi^2} \ln \left(\frac{M_{X_1}^2}{m_t^2} \right). \tag{2.48}
\end{aligned}$$

Finally, to correct for the photon we left off, we need to multiply by the top quark charge, $\frac{2}{3}$ and a factor of $\frac{1}{2}$ since this amplitude is generated by both terms in $F^{\mu\nu}$. This gives our desired result,

$$i \frac{d_d}{2} = i \frac{m_t}{12\pi^2 M_{X_1}^2} \ln \left(\frac{M_{X_1}^2}{m_t^2} \right) \text{Im}(g_1^{13} g_1'^{31*}) \tag{2.49}$$

2.C K^0 - \bar{K}^0 mixing

Here, we show explicitly the transformation between 2-component and 4-component notation for the effective Hamiltonian in K^0 - \bar{K}^0 mixing. We start by writing the spinor indices,

$$\begin{aligned}
\mathcal{H}_{\text{eff}} &= \frac{g_2^{22} (g_2^{11})^*}{M_2^2} (s_{R\alpha} s_{R\beta}) (d_R^{*\alpha} d_R^{*\beta}) \\
&= \frac{g_2^{22} (g_2^{11})^*}{M_2^2} (s_{R\alpha}^{\dot{a}} \epsilon_{\dot{a}b} s_{R\beta}^{\dot{b}}) (d_R^{*\alpha a} \epsilon_{ab} d_R^{*\beta b}). \tag{2.50}
\end{aligned}$$

Next, we use the identity $2\epsilon_{\dot{a}b}\epsilon_{ab} = \sigma_{\dot{a}a}^\mu \sigma_{\mu bb}$ to write this as

$$\begin{aligned}
&= \frac{g_2^{22} (g_2^{11})^*}{2M_2^2} (s_{R\alpha}^{\dot{a}} s_{R\beta}^{\dot{b}} d_R^{*\alpha a} d_R^{*\beta b}) \sigma_{\dot{a}a}^\mu \sigma_{\mu bb} \\
&= \frac{g_2^{22} (g_2^{11})^*}{2M_2^2} (d_R^{*\alpha a} \sigma_{\dot{a}a}^\mu s_{R\alpha}^{\dot{a}}) (d_R^{*\beta b} \sigma_{\mu bb} s_{R\beta}^{\dot{b}}) \\
&= \frac{g_2^{22} (g_2^{11})^*}{2M_2^2} (\bar{d}_R^\alpha \gamma^\mu s_{R\alpha}) (\bar{d}_R^\beta \gamma_\mu s_{R\beta}) \tag{2.51}
\end{aligned}$$

where the last line is in 4-component notation.

2.D Absorptive part of X_2 decay

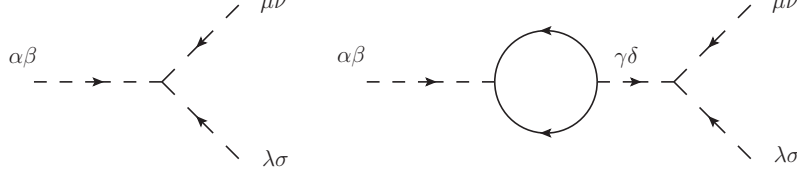


Figure 2.D.1: Color structure of the relevant diagrams for X_2 decay.

We start with the tree-level diagram in Fig. 2.D.1. The Feynman rule for this vertex gives

$$i\mathcal{M}_{\text{tree}} = 2i\epsilon_{\alpha\mu\lambda}\epsilon_{\beta\nu\sigma} . \quad (2.52)$$

Because the same color structure appears in the 1-loop diagram, it will be useful to compute the decay amplitude for the tree-level process.

$$\begin{aligned} \Gamma_{\text{tree}} &= \frac{1}{2} \frac{1}{16\pi M_2} \frac{1}{6} \sum_{\text{initial colors}} \frac{1}{2} \left(\delta_{\alpha'}^{\alpha} \delta_{\beta'}^{\beta} + \delta_{\beta'}^{\alpha} \delta_{\alpha'}^{\beta} \right) \sum_{\text{final colors}} \frac{1}{4} \left(\delta_{\mu'}^{\mu} \delta_{\nu'}^{\nu} + \delta_{\nu'}^{\mu} \delta_{\mu'}^{\nu} \right) \left(\delta_{\lambda'}^{\lambda} \delta_{\sigma'}^{\sigma} + \delta_{\sigma'}^{\lambda} \delta_{\lambda'}^{\sigma} \right) \\ &\quad \times 4|\lambda|^2 \epsilon_{\alpha\mu\lambda} \epsilon_{\beta\nu\sigma} \epsilon^{\alpha'\mu'\lambda'} \epsilon^{\beta'\nu'\sigma'} \\ &= \frac{3}{8\pi M_2} |\lambda|^2 \end{aligned} \quad (2.53)$$

The factors involving δ 's are used to symmetrize the amplitude over symmetric color indices, the factors of $\frac{1}{2}$ is for identical final states, and the factors of $\frac{1}{6}$ is for averaging over initial colors.

Next, we include the amplitude coming from the loop-diagram. The amplitude is

$$i\mathcal{M}_{\text{loop}} = 2\lambda' \text{Tr}[\tilde{g}_2^\dagger g_2] \epsilon_{\alpha\mu\lambda} \epsilon_{\beta\nu\sigma} \frac{1}{M_2^2 - \tilde{M}_2^2} I(p^2) \quad (2.54)$$

where the $I(p^2)$ is the loop factor

$$\begin{aligned}
I(p^2) &= 2 \int \frac{d^4 q}{(2\pi)^4} \text{Tr} \left[\frac{i\not{q}}{q^2 + i\epsilon} P_R \frac{(-i)(\not{p} + \not{q})}{(p+q)^2 + i\epsilon} \right] \\
&= -2 \int \frac{d^4 q}{(2\pi)^4} \frac{1}{q^2 + i\epsilon} \frac{1}{(p+q)^2 + i\epsilon} \text{Tr} [(-\not{q}) P_R (\not{p} + \not{q})] \\
&= -2 \int \frac{d^4 q}{(2\pi)^4} \frac{1}{q^2 + i\epsilon} \frac{1}{(p+q)^2 + i\epsilon} 2q_1 \cdot q_2
\end{aligned} \tag{2.55}$$

where we've defined $q_1 = -q$ and $q_2 = p + q$. Now, the difference in decay rates between X_2 and \bar{X}_2 will depend only on the imaginary part of this loop integral which we can compute using the usual Cutkosky rules.

$$\begin{aligned}
\text{Disc} [I(p^2)] &= -2 \int \frac{d^4 q_1}{(2\pi)^4} \frac{d^4 q_2}{(2\pi)^4} (2\pi)^4 \delta^{(4)}(q_1 + q_2 - p) (-2\pi i) \delta(q_1^2) (-2\pi i) \delta(q_2^2) 2q_1 \cdot q_2 \\
&= 16\pi^2 \int \frac{d^4 q_1}{(2\pi)^4} \delta(q_1^2) \delta[(p - q_1)^2] \frac{M_2^2}{2} \\
&= \frac{16\pi^2 M_2^2}{2(2\pi)^4} \int d^4 q_1 \frac{\delta(q_1^0 - |\vec{q}_1|)}{2q_1^0} \frac{\delta(\frac{M_2}{2} - q_1^0)}{2M_2} \\
&= \frac{16\pi^2 M_2^2}{2(2\pi)^4} \int d^3 \vec{q}_1 \frac{\delta(\frac{M_2}{2} - |\vec{q}_1|)}{M_2} \frac{1}{2M_2} \\
&= \frac{16\pi^2}{4(2\pi)^4} \int 4\pi |\vec{q}_1|^2 d|\vec{q}_1| \delta(\frac{M_2}{2} - |\vec{q}_1|) \\
&= \frac{16\pi^3}{(2\pi)^4} \left(\frac{M_2}{2} \right)^2 \\
&= \frac{M_2^2}{4\pi}
\end{aligned} \tag{2.56}$$

In the second line, we've integrated over q_2 to eliminate the $\delta^{(4)}$. In the third line, we've used an identity to rewrite the composition of a Dirac delta and another function.

Now, we use the fact that $\text{Disc} [I(p^2)] = 2i \text{Im} [I(p^2)]$ to get the relevant part of our amplitude

$$i\mathcal{M}_{\text{loop}} = -2i\lambda' \text{Tr}[\tilde{g}_2^\dagger g_2] \epsilon_{\alpha\mu\lambda} \epsilon_{\beta\nu\sigma} \frac{1}{M_2^2 - \tilde{M}_2^2} \frac{M_2^2}{8\pi}. \tag{2.57}$$

Comparing this to our tree-level result tells us that

$$\begin{aligned} \Gamma &= \frac{3}{8\pi M_2} \left| \lambda - i\lambda' \text{Tr}[\tilde{g}_2^\dagger g_2] \frac{1}{M_2^2 - \tilde{M}_2^2} \frac{M_2^2}{8\pi} \right|^2 \\ &\simeq \frac{3\lambda}{8\pi M_2} \left[\lambda - \lambda' \frac{M_2^2}{4\pi(M_2^2 - \tilde{M}_2^2)} \text{Im}(\text{Tr}(g_2^\dagger \tilde{g}_2)) \right]. \end{aligned} \quad (2.58)$$

Chapter 3

Phenomenology of scalar leptoquarks

3.1 Introduction

Currently, the standard model describes most aspects of nature with remarkable precision. If there is new physics at the multi TeV scale (perhaps associated with the hierarchy puzzle), it is reasonable to expect measurable deviations from the predictions of the standard model in the flavor sector. Amongst the experiments with very high reach in the mass scale associated with beyond the standard model physics are those that look for flavor violation in the charged lepton sector through measurements of the processes, $\mu \rightarrow e\gamma$ [29] and $\mu \rightarrow e$ conversion [30, 31], and the search for electric dipole moments of the neutron, proton and electron.

Models with scalar leptoquarks can modify the rates for these processes. Simple models of this type have been studied previously in the literature, including their classification and phenomenology [32, 33, 34, 35, 36, 37, 38, 39].

Our approach is to first identify the minimal renormalizable scalar leptoquark models containing one single additional representation of $SU(3) \times SU(2) \times U(1)$ and construct the most general renormalizable model without any additional constraints on the couplings apart from the usual ones, i.e., gauge invariance, Poincaré invariance, and locality. Given the strong experimental constraints on baryon number violating processes like $p \rightarrow \pi^0 e^+$, we concentrate only on those scalar leptoquark models which don't have baryon number

violation in perturbation theory via leptoquark exchange. Of course there is baryon number violation through non-perturbative quantum effects since it is an anomalous symmetry. But this is a very small effect at zero temperature. Only two models fulfill this requirement. One of those two models gives a top mass enhanced $\mu \rightarrow e\gamma$ decay rate. We perform an analysis of the phenomenology of this specific model, including the $\mu \rightarrow e\gamma$ decay rate, $\mu \rightarrow e$ conversion rate, as well as electric dipole moment constraints focussing mostly on the regions of parameter space where the impact of the top quark mass enhancement is most important. For lepton flavor violating processes at higher energies such as $\tau \rightarrow \mu\gamma$, deep inelastic scattering $e + p \rightarrow \mu(\tau) + X$, *etc.*, the impact on the phenomenology of the top quark mass enhancement of charged lepton chirality flip is less dramatic and that is why we focus in this paper on low energy processes involving the lightest charged leptons.

We also consider the effects of dimension five operators that can cause baryon number violation. We find that the two models without renormalizable baryon number violation can have such operators and, even if the operators are suppressed by the Planck scale, they may (depending on the values of coupling constants and masses) give rise to an unacceptable level of baryon number violation. We discuss a way to forbid these dimension five operators.

3.2 Models

A general classification of renormalizable leptoquark models can be found in [32, 33]. However, in the spirit of our approach, in which we are interested in models with no proton decay from leptoquark exchange, a more useful list of possible interaction terms between the scalar leptoquarks and fermion bilinears is presented in [40], where those models that have tree-level proton decay are highlighted. The relevant models are listed in Table 3.1 below.

The only two models fulfilling our requirement are $X = (3, 2, 7/6)$ and $X = (3, 2, 1/6)$

leptoquark couplings	diquark couplings	$SU(3) \times SU(2) \times U(1)$ representation of X
$XQe, XL\bar{u}$	–	$(3, 2, 7/6)$
XLd	–	$(3, 2, 1/6)$
$XQL, X\bar{u}\bar{e}$	XQQ, Xud	$(3, 1, -1/3)_{\text{PD}}$
XQL	XQQ	$(3, 3, -1/3)_{\text{PD}}$
$Xd\bar{e}$	Xuu	$(3, 1, -4/3)_{\text{PD}}$

Table 3.1: Possible interaction terms between the scalar leptoquarks and fermion bilinears along with the corresponding quantum numbers. Representations labeled with the subscript ‘‘PD’’ allow for proton decay via tree-level scalar exchange.

Model I: $X = (3, 2, 7/6)$.

The Lagrangian for the scalar leptoquark couplings to the fermion bilinears in this model is,

$$\mathcal{L} = -\lambda_u^{ij} \bar{u}_R^i X^T \epsilon L_L^j - \lambda_e^{ij} \bar{e}_R^i X^\dagger Q_L^j + \text{h.c.}, \quad (3.1)$$

where,

$$X = \begin{pmatrix} V_\alpha \\ Y_\alpha \end{pmatrix}, \quad \epsilon = \begin{pmatrix} 0 & 1 \\ -1 & 0 \end{pmatrix}, \quad L_L = \begin{pmatrix} \nu_L \\ e_L \end{pmatrix}. \quad (3.2)$$

After expanding the $SU(2)$ indices it takes the form,

$$\mathcal{L} = -\lambda_u^{ij} \bar{u}_{\alpha R}^i (V_\alpha e_L^j - Y_\alpha \nu_L^j) - \lambda_e^{ij} \bar{e}_R^i (V_\alpha^\dagger u_{\alpha L}^j + Y_\alpha^\dagger d_{\alpha L}^j) + \text{h.c.}. \quad (3.3)$$

Note that in this model the left-handed charged lepton fields couple to right-handed top quarks, and the right-handed charged lepton fields couple to left-handed top quarks. So a charged lepton chirality flip can be caused by the top mass at one loop.

Model II: $X = (3, 2, 1/6)$.

The corresponding Lagrangian is,

$$\mathcal{L} = -\lambda_d^{ij} \bar{d}_R^i X^T \epsilon L_L^j + \text{h.c.} , \quad (3.4)$$

where we have used the same notation as in the previous case. Expanding the $SU(2)$ indices yields,

$$\mathcal{L} = -\lambda_d^{ij} \bar{d}_{\alpha R}^i (V_\alpha e_L^j - Y_\alpha \nu_L^j) + \text{h.c.} . \quad (3.5)$$

In model II the leptoquark cannot couple to the top quark, so there is no m_t enhancement in the $\mu \rightarrow e\gamma$ decay rate. There is also no m_b enhancement, and the one-loop effective Hamiltonian for $\mu \rightarrow e\gamma$ (after integrating out the massive scalars and the heavy quarks) is proportional to the muon mass. In addition, as mentioned in [40], this model does generate tree-level proton decay from its interaction with the Higgs field. For this reason, in the remainder of the paper we will focus entirely on model I.

3.3 Phenomenology

In this section we analyze some of the phenomenology of model I, i.e., $X = (3, 2, 7/6)$. We concentrate only on those constraints which are most restrictive for the model and potentially most sensitive to the unusual top mass enhancement of the charged lepton chirality change, i.e., the ones coming from the following processes – muon decay to an electron and a photon, muon to electron conversion, and electric dipole moment of the electron.

3.3.1 Naturalness

Before elaborating on the phenomenology of the model, we first discuss the range of couplings allowed by the naturalness criterion. The contribution to the charged lepton mass

matrix induced at one loop is given by,

$$\Delta m_{ij} \simeq \tilde{\lambda}_u^{3i} \tilde{\lambda}_e^{j3} \frac{3m_t}{16\pi^2} \log\left(\frac{\Lambda^2}{m_V^2}\right), \quad (3.6)$$

where Λ is the cut-off scale. To avoid unnatural cancellations between this loop contribution to the lepton mass matrix and the tree-level lepton mass matrix we require,

$$|\Delta m_{ij}| \lesssim \sqrt{m_i m_j}. \quad (3.7)$$

For example, for a scalar of mass $m_V = 50$ TeV and a cut-off set at the GUT scale Eq. (3.6) gives,

$$\Delta m_{ij} \simeq \tilde{\lambda}_u^{3i} \tilde{\lambda}_e^{j3} \times 170 \text{ GeV}, = \quad (3.8)$$

which, combined with Eq. (3.7), yields the following constraint on the couplings,

$$|\tilde{\lambda}_e^{13} \tilde{\lambda}_u^{32}|, |\tilde{\lambda}_e^{23} \tilde{\lambda}_u^{31}| \lesssim 4.3 \times 10^{-5}. \quad (3.9)$$

In the subsequent analysis we will include the constraint imposed by Eq. (3.7) by indicating which region of the plots is not favored by the naturalness considerations.

3.3.2 $\mu \rightarrow e\gamma$ decay

The relevant Feynman diagrams for this process are presented in Fig. 3.1. The uniqueness of model I is that, apart from the fact there is no tree-level proton decay, the $\mu \rightarrow e\gamma$ rate is enhanced by the top quark mass. To our knowledge, such an enhancement of $\mu \rightarrow e\gamma$ was observed previously only in [36] in the context of an $SU(2)$ singlet scalar leptoquark model. However, that model suffers from perturbative proton decay and the impact of the m_t enhancement was not focussed on.

Keeping only the piece enhanced by m_t , the sum of amplitudes corresponding to the

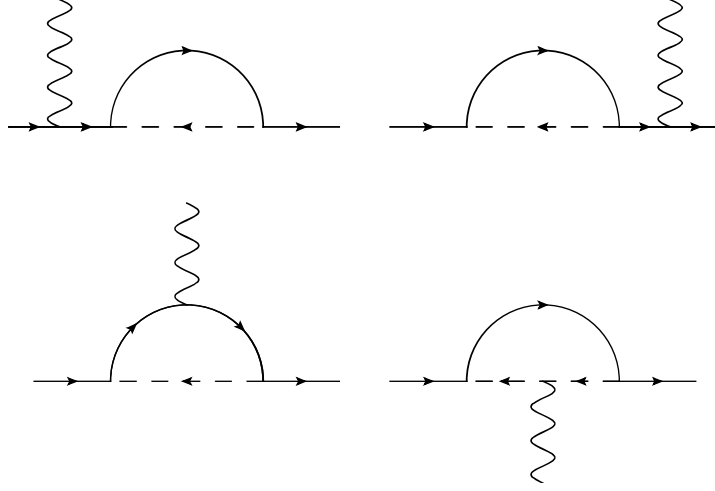


Figure 3.1: Feynman diagrams contributing to the process $\mu \rightarrow e\gamma$.

diagrams in Fig. 3.1 (neglecting the terms proportional to m_e) is given by (see Appendix 3.A),

$$i\mathcal{M} = -\frac{3e m_t}{16\pi^2 m_V^2} f(m_t^2/m_V^2) k_\nu \epsilon_\mu(k) \times \left[\tilde{\lambda}_e^{13} \tilde{\lambda}_u^{32} \bar{e}_R(p-k) \sigma^{\mu\nu} \mu_L(p) + (\tilde{\lambda}_u^{31})^* (\tilde{\lambda}_e^{23})^* \bar{e}_L(p-k) \sigma^{\mu\nu} \mu_R(p) \right], \quad (3.10)$$

where k is the photon four-momentum and ϵ is the photon polarization. The function $f(m_t^2/m_V^2)$ is given by,

$$f(x) = \frac{1-x^2+2x\log x}{2(1-x)^3} + \frac{2}{3} \left(\frac{1-x+\log x}{(1-x)^2} \right), \quad (3.11)$$

and the tilde over the couplings denotes that they are related by transformations that take the quarks and leptons to their mass eigenstate basis through the following 3×3 matrix transformations,

$$\tilde{\lambda}_u = U(u, R)^\dagger \lambda_u U(e, L), \quad \tilde{\lambda}_e = U(e, R)^\dagger \lambda_e U(u, L), \quad (3.12)$$

where the right-handed up quarks in the Lagrangian are related to the right-handed mass

eigenstate up-type quarks by the matrix $U(u, R)$, the left-handed up quarks in the Lagrangian are related to the left-handed mass eigenstate up-type quarks by the matrix $U(u, L)$, *etc.*

The $\mu \rightarrow e\gamma$ decay rate is,

$$\Gamma(\mu \rightarrow e\gamma) = \frac{9e^2\lambda^2 m_t^2 m_\mu^3}{2048\pi^5 m_V^4} f(m_t^2/m_V^2)^2, \quad (3.13)$$

where,

$$\lambda \equiv \sqrt{\frac{1}{2}|\tilde{\lambda}_e^{13}\tilde{\lambda}_u^{32}|^2 + \frac{1}{2}|\tilde{\lambda}_u^{31}\tilde{\lambda}_e^{23}|^2}. \quad (3.14)$$

Fig. 3.2 shows the relation between λ and the scalar leptoquark mass. This dependence was plotted for the $\mu \rightarrow e\gamma$ branching ratio equal to the current upper limit of $\text{Br}(\mu \rightarrow e\gamma) \simeq 2.4 \times 10^{-12}$ reported by the MEG experiment, and the prospective MEG sensitivity of $\text{Br}(\mu \rightarrow e\gamma) \simeq 5.0 \times 10^{-13}$. It shows that the experiment will be sensitive to scalar leptoquark masses at the hundred TeV scale for small values of the couplings.

For very small x , $f(x) \rightarrow \tilde{f}(x) = \frac{2}{3} \log x$. This is a reasonable approximation in the range of x we are interested in. For example, $\tilde{f}(10^{-8})/f(10^{-8}) \simeq 1.1$.

3.3.3 $\mu \rightarrow e$ conversion

The effective Hamiltonian for the $\mu \rightarrow e$ conversion arises from two sources,

$$\mathcal{H}_{\text{eff}} = \mathcal{H}_{\text{eff}}^{(a)} + \mathcal{H}_{\text{eff}}^{(b)}. \quad (3.15)$$

The first is the dipole transition operator that comes from the loop diagrams which are responsible for the $\mu \rightarrow e\gamma$ decay, given by,

$$\begin{aligned} \mathcal{H}_{\text{eff}}^{(a)} &= \frac{3em_t}{32\pi^2 m_V^2} f(m_t^2/m_V^2) \\ &\times \left[\tilde{\lambda}_e^{13}\tilde{\lambda}_u^{32} \bar{e}_R \sigma_{\mu\nu} \mu_L F^{\mu\nu} + (\tilde{\lambda}_u^{31})^* (\tilde{\lambda}_e^{23})^* \bar{e}_L \sigma_{\mu\nu} \mu_R F^{\mu\nu} \right]. \end{aligned} \quad (3.16)$$

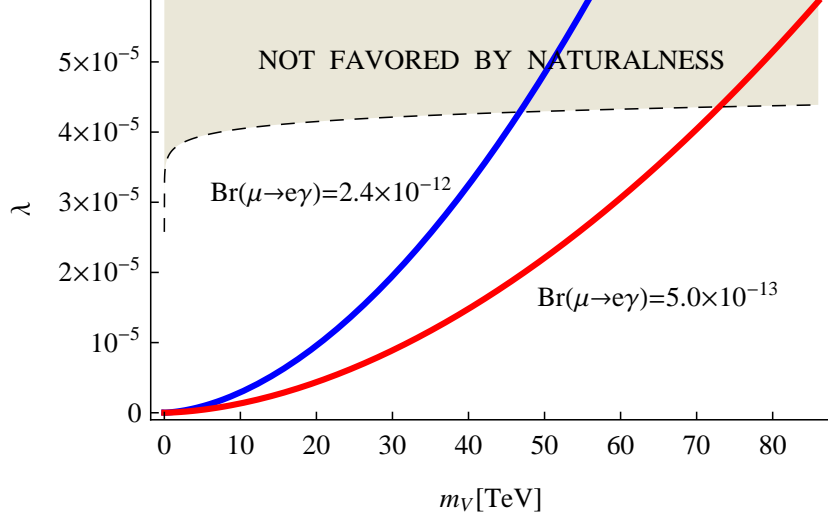


Figure 3.2: The combination of couplings λ from Eq. (3.14) as a function of the scalar leptoquark mass for two values of the $\mu \rightarrow e\gamma$ branching ratio relevant for the MEG experiment. The shaded region consists of points which do not satisfy Eq. (3.7).

Using the following Fierz identities (for spinors),

$$\begin{aligned}
(\bar{u}_{1L}u_{2R})(\bar{u}_{3R}u_{4L}) &= \frac{1}{2}(\bar{u}_{1L}\gamma^\mu u_{4L})(\bar{u}_{3R}\gamma_\mu u_{2R}), \\
(\bar{u}_{1L}u_{2R})(\bar{u}_{3L}u_{4R}) &= \frac{1}{2}(\bar{u}_{1L}u_{4R})(\bar{u}_{3L}u_{2R}) \\
&+ \frac{1}{8}(\bar{u}_{1L}\sigma^{\mu\nu}u_{4R})(\bar{u}_{3R}\sigma_{\mu\nu}u_{2L}),
\end{aligned} \tag{3.17}$$

we arrive, after integrating out the heavy scalar leptoquarks (at tree level), at the second part of the effective Hamiltonian,

$$\begin{aligned}
\mathcal{H}_{\text{eff}}^{(b)} &= \frac{1}{2m_V^2} \left\{ \tilde{\lambda}_u^{12}(\tilde{\lambda}_u^{11})^*(\bar{e}_L\gamma^\mu\mu_L)(\bar{u}_{\alpha R}\gamma_\mu u_{\alpha R}) \right. \\
&+ \tilde{\lambda}_e^{11}\tilde{\lambda}_u^{12} \left[C_S(\mu)(\bar{e}_R\mu_L)(\bar{u}_{\alpha R}u_{\alpha L}) + \frac{1}{4}C_T(\mu)(\bar{e}_R\sigma^{\mu\nu}\mu_L)(\bar{u}_{\alpha R}\sigma_{\mu\nu}u_{\alpha L}) \right] \\
&+ \tilde{\lambda}_e^{11}(\tilde{\lambda}_e^{21})^*(\bar{e}_R\gamma^\mu\mu_R)(\bar{u}_{\alpha L}\gamma_\mu u_{\alpha L}) \\
&+ \left. (\tilde{\lambda}_e^{21})^*(\tilde{\lambda}_u^{11})^* \left[C_S(\mu)(\bar{e}_L\mu_R)(\bar{u}_{\alpha L}u_{\alpha R}) + \frac{1}{4}C_T(\mu)(\bar{e}_L\sigma^{\mu\nu}\mu_R)(\bar{u}_{\alpha L}\sigma_{\mu\nu}u_{\alpha R}) \right] \right\} \\
&+ \frac{1}{2m_Y^2}(\tilde{\lambda}_e V_{CKM})^{11} \left((\tilde{\lambda}_e V_{CKM})^{21} \right)^* (\bar{e}_R\gamma^\mu\mu_R)(\bar{d}_{\alpha L}\gamma_\mu d_{\alpha L}) + \dots \tag{3.18}
\end{aligned}$$

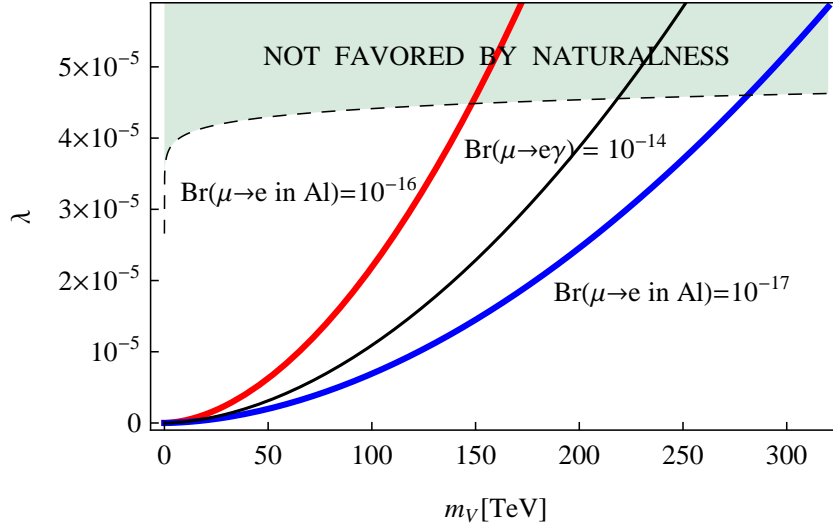


Figure 3.3: The combination of couplings λ from Eq. (3.14) as a function of the scalar leptoquark mass for two values of the $\text{Br}(\mu \rightarrow e$ conversion in Al) relevant for the Mu2e experiment. The thin solid line, corresponding to $\text{Br}(\mu \rightarrow e\gamma) = 10^{-14}$, is included for reference. The shaded region consists of points which do not satisfy Eq. (3.7).

The CKM matrix arises whenever a coupling to the left-handed down-type quark appears. In Eq. (3.18) the contribution of the heavy quarks, as well as the contribution of the strange quark, are in the ellipses. Since the operators $\bar{q}q$ and $\bar{q}\sigma^{\mu\nu}q$ do require renormalization, their matrix elements develop subtraction point dependence that is cancelled in the leading logarithmic approximation by that of the coefficients $C_{S,T}$. Including strong interaction leading logarithms we get,

$$C_S(\mu) = \left[\frac{\alpha_s(m_V)}{\alpha_s(\mu)} \right]^{-12/(33-2N_q)} \quad (3.19)$$

and

$$C_T(\mu) = \left[\frac{\alpha_s(m_V)}{\alpha_s(\mu)} \right]^{4/(33-2N_q)}, \quad (3.20)$$

where $N_q = 6$ is the number of quarks with mass below m_V . In order to match the effective Hamiltonian (3.18) to the Hamiltonian at the nucleon level and use this to compute the conversion rate, we follow the steps outlined in [41, 42].

Our results, taking into account only the contribution from $\mathcal{H}_{\text{eff}}^{(a)}$, are shown in Fig. 3.3.

The current experimental limit is $\text{Br}(\mu \rightarrow e \text{ conversion in Au}) < 7.0 \times 10^{-13}$ [43]. However, here we focus on the prospective Mu2e experiment [30], which has a sensitivity goal of 5×10^{-17} . The COMET experiment [31] aims for comparable sensitivity in later stages. We use the total capture rate for $^{27}_{13}\text{Al}$ of $\omega_{\text{capture}} = 0.7054 \times 10^6 \text{ s}^{-1}$ [44] to switch from the $\mu \rightarrow e$ conversion rate to a branching ratio.

Apart from coupling constant factors, the contribution to the $\mu \rightarrow e$ conversion amplitude from $\mathcal{H}_{\text{eff}}^{(a)}$ is enhanced over the contribution to the amplitude from $\mathcal{H}_{\text{eff}}^{(b)}$ roughly by $(m_t/m_\mu)(3e^2/32\pi^2) \log(m_V^2/m_t^2) \sim 10$, for m_V in the hundred TeV range.

Our results show that in some regions of parameter space the Mu2e experiment will be able to constrain leptoquark couplings with similar precision to what can be done with an experiment which is sensitive to a branching ratio for $\mu \rightarrow e\gamma$ of around 10^{-14} . In other regions the Mu2e experiment is likely to give a more powerful constraint for such a $\mu \rightarrow e\gamma$ branching ratio, for example, when the Yukawa couplings are strongly hierarchical and the top quark loop is very suppressed.

To show graphically the contributions to the branching ratio originating from terms in the effective Hamiltonian with different structures, we set all the couplings to zero apart from $\tilde{\lambda}_e^{13}, \tilde{\lambda}_e^{23}, \tilde{\lambda}_u^{31}, \tilde{\lambda}_u^{32}, \tilde{\lambda}_u^{11}, \tilde{\lambda}_u^{12}$ for simplicity, i.e., we leave only the couplings relevant for the $\mu \rightarrow e\gamma$ decay and one of the vector contributions to $\mathcal{H}_{\text{eff}}^{(b)}$.

Note that the heavy quark contributions are suppressed by Λ_{QCD}/m_Q , low energy phenomenology suggests that the strange quark contribution is small, and furthermore the tensor contributions are not enhanced by the atomic number of the target.

In addition, we consider only real couplings and define $\kappa \equiv \tilde{\lambda}_u^{11}\tilde{\lambda}_u^{12}$. We also assume $\tilde{\lambda}_e^{13}\tilde{\lambda}_u^{32} = \tilde{\lambda}_u^{31}\tilde{\lambda}_e^{23} = \lambda$, so that we can plot λ as a function of the scalar leptoquark mass m_V for a given value of the ratio,

$$r \equiv \frac{\kappa}{\lambda} = \frac{\tilde{\lambda}_u^{11}\tilde{\lambda}_u^{12}}{\sqrt{\frac{1}{2}(\tilde{\lambda}_e^{13}\tilde{\lambda}_u^{32})^2 + \frac{1}{2}(\tilde{\lambda}_u^{31}\tilde{\lambda}_e^{23})^2}}. \quad (3.21)$$

Figs. 3.4, 3.5, 3.6, and 3.7 show our results for a few values of $r = \pm 1, \pm 10, \pm 100, \pm 200$

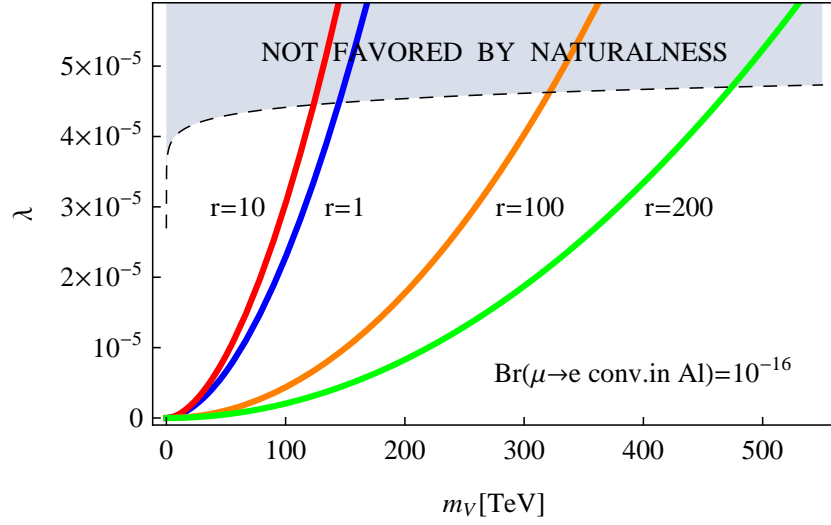


Figure 3.4: The combination of couplings λ from Eq. (3.14) as a function of the scalar leptoquark mass for a branching ratio $\text{Br}(\mu \rightarrow e \text{ conversion in AI}) = 10^{-16}$ and four different positive values of the ratio of the couplings r from Eq. (3.21). The shaded region consists of points which do not satisfy Eq. (3.7).

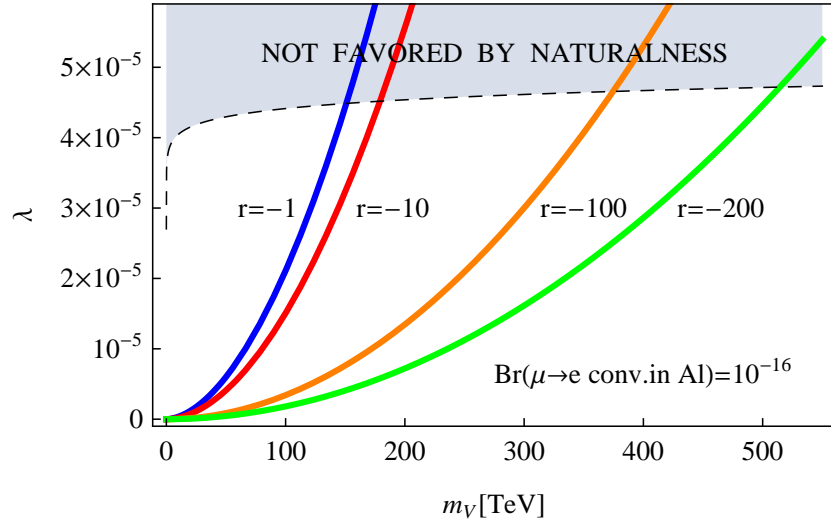


Figure 3.5: Same as Fig. 3.4, but for negative values of r .

and two values of the branching ratio $\text{Br}(\mu \rightarrow e \text{ conversion in AI}) = 10^{-16}, 10^{-17}$.

For $r \lesssim 1$ the branching ratio is dominated by the $\mathcal{H}_{\text{eff}}^{(a)}$ contribution and in this parameter region all curves look like the ones in Fig. 3.3. For larger values of r , depending on the relative sign between the contributions from $\mathcal{H}_{\text{eff}}^{(a)}$ and $\mathcal{H}_{\text{eff}}^{(b)}$, there are two possibilities.

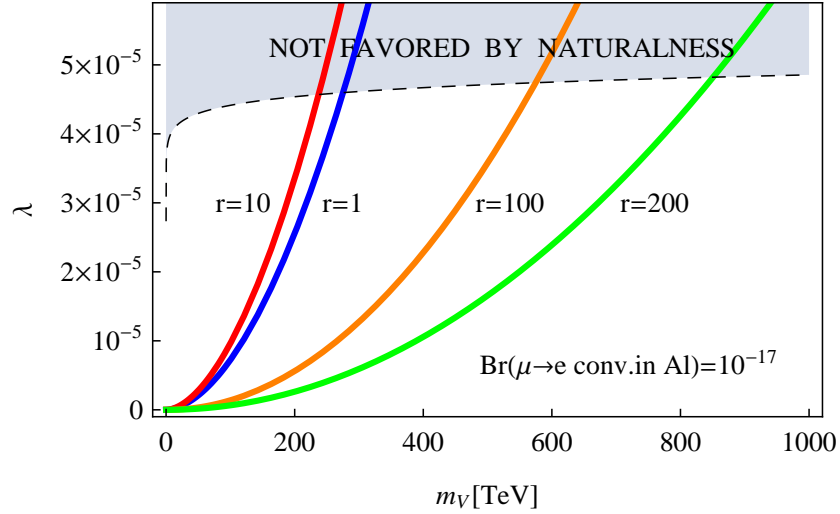


Figure 3.6: Same as Fig. 3.4, but for a branching ratio $\text{Br}(\mu \rightarrow e \text{ conversion in Al}) = 10^{-17}$.

If the interference is constructive, the curve moves down with increasing r since a smaller value of the coupling λ is required to achieve a given branching ratio (Figs. 3.5 and 3.7). In the case of a destructive interference, the curves move up until a value of r is reached for which the two contributions are the same (Figs. 3.4 and 3.6). As estimated before, this occurs for $r \approx 10$. Increasing r further brings the curves back down, since the $\mathcal{H}_{\text{eff}}^{(b)}$ contribution becomes dominant.

Large values of r are expected if the Yukawa couplings of X exhibit a hierarchical pattern like what is observed in the quark sector; κ changes generations by one unit while the product of couplings in λ involves changing generations by three units. Finally, we note that for all the curves in the plots above the Yukawa couplings are well within the perturbative regime.

3.3.4 Electron EDM

Another flavor constraint on the couplings of model I comes from the electric dipole moment (EDM) of the electron. As mentioned earlier, the fact that X couples directly to both left- and right-handed quarks means that at one loop the top quark mass can induce the

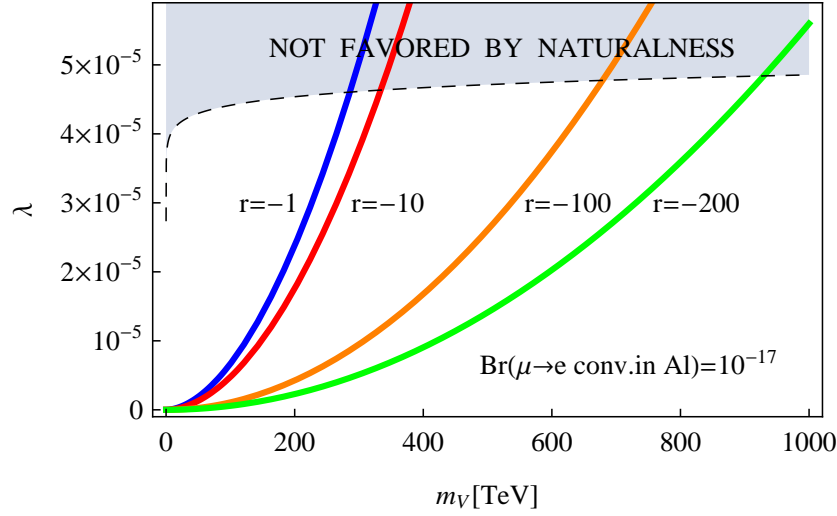


Figure 3.7: Same as Fig. 3.5, but for a branching ratio $\text{Br}(\mu \rightarrow e \text{ conversion in Al}) = 10^{-17}$.

chirality flip necessary to give an electron EDM. We find that,

$$|d_e| \simeq \frac{3 e m_t}{16 \pi^2 m_V^2} f(m_t^2/m_V^2) |\text{Im}[\tilde{\lambda}_e^{13} \tilde{\lambda}_u^{31}]|. \quad (3.22)$$

The present electron EDM experimental limit [45] is,

$$|d_e| < 10.5 \times 10^{-28} e \text{ cm}. \quad (3.23)$$

We can write the dipole moment in terms of the branching ratio, $\text{Br}(\mu \rightarrow e \gamma)$, giving the constraint

$$\frac{|\text{Im}[\tilde{\lambda}_e^{13} \tilde{\lambda}_u^{31}]|}{\lambda} \sqrt{\text{Br}(\mu \rightarrow e \gamma)} < 2.0 \times 10^{-7}. \quad (3.24)$$

For example, if model I gave a branching ratio equal to the current experimental bound of $\text{Br}(\mu \rightarrow e \gamma) < 2.4 \times 10^{-12}$, this would correspond to the constraint on the couplings of $|\text{Im}[\tilde{\lambda}_e^{13} \tilde{\lambda}_u^{31}]|/\lambda < 0.13$. Fig. 3.8 shows the relation between the parameters $|\text{Im}[\tilde{\lambda}_e^{13} \tilde{\lambda}_u^{31}]|$ and m_V for the electron EDM equal to $|d_e| = 10^{-27}$, 10^{-28} , and $10^{-29} e \text{ cm}$.

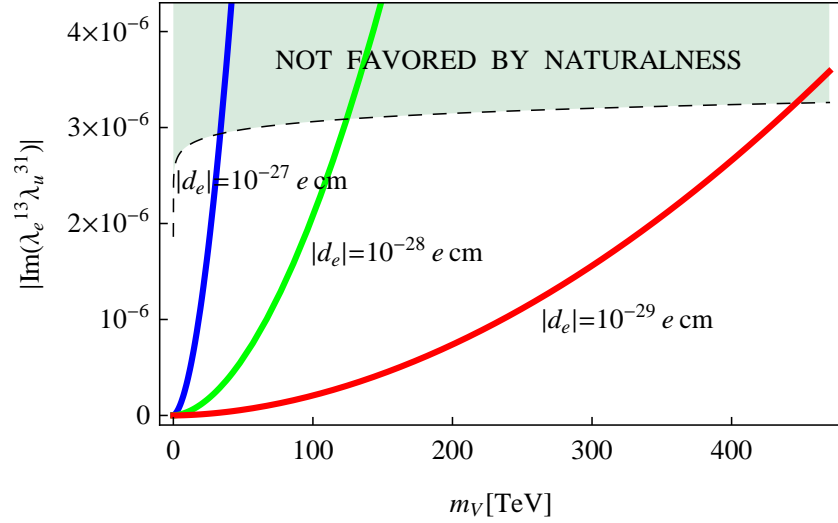


Figure 3.8: The combination of couplings $|\text{Im}[\tilde{\lambda}_e^{13} \tilde{\lambda}_u^{31}]|$ as a function of the scalar leptoquark mass for three different values of the electron EDM. The shaded region consists of points which do not satisfy Eq. (3.7).

3.4 Baryon number violation and dimension five operators

Tree-level renormalizable interactions are not the only possible source of baryon number violation. It might also occur through higher-dimensional nonrenormalizable operators. In the standard model, proton decay is restricted to operators of mass dimension six or higher. However, the scalar leptoquark models we consider exhibit proton decay through dimension five operators.

Let's first consider model I, in which $X = (3, 2, 7/6)$. Although it doesn't give proton decay at tree level, one can construct the following dimension five operator,

$$\mathcal{O}_I = \frac{1}{\Lambda} g^{ab} d_{R\alpha}^a d_{R\beta}^b (H^\dagger X_\gamma) \epsilon^{\alpha\beta\gamma}. \quad (3.25)$$

The coupling constant matrix g is antisymmetric in flavor space. Because of the tree-level leptoquark couplings (see, Table 3.1), baryon number violating decay occurs here through the process shown in Fig. 3.9, resulting in $n \rightarrow e^- K^+$ and $p \rightarrow K^+ \nu$. Setting the coupling

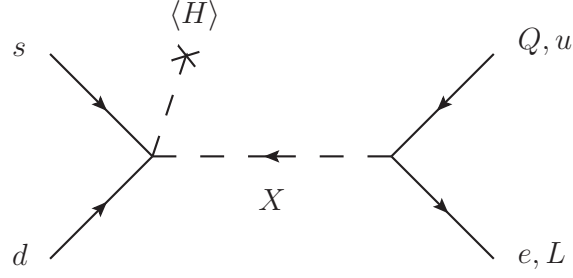


Figure 3.9: Feynman diagram representing proton decay in model I.

constants to unity, we estimate the baryon number violating nucleon decay rate caused by this operator to be,

$$\Gamma_p \approx 2 \times 10^{-57} \left(\frac{50 \text{ TeV}}{m_V} \right)^4 \left(\frac{M_{\text{PL}}}{\Lambda} \right)^2 \text{ GeV}. \quad (3.26)$$

Since the current experimental limit is $\Gamma_p^{\text{exp}} < 2.7 \times 10^{-66} \text{ GeV}$ [46], even if the scale of new physics Λ is equal to the Planck mass M_{PL} when the coupling constants are unity, this operator causes too large a proton decay rate for $m_V \lesssim 10\,000 \text{ TeV}$.

In the case of model II, where $X = (3, 2, 1/6)$, there are two dimension five baryon number violating operators,

$$\begin{aligned} \mathcal{O}_{II}^{(1)} &= \frac{1}{\Lambda} g^{ab} u_{R\alpha}^a d_{R\beta}^b (H^\dagger X_\gamma) \epsilon^{\alpha\beta\gamma}, \\ \mathcal{O}_{II}^{(2)} &= \frac{1}{\Lambda} g^{ab} u_{R\alpha}^a e_R^b (X_\beta \epsilon X_\gamma) \epsilon^{\alpha\beta\gamma}. \end{aligned} \quad (3.27)$$

The operator $\mathcal{O}_{II}^{(1)}$ permits a nucleon decay pattern similar to the previous case, e.g., $n \rightarrow e^- \pi^+$ and $p \rightarrow \pi^+ \nu$. Proton decay through the operator $\mathcal{O}_{II}^{(2)}$ is much more suppressed.

In order to prevent proton decay through dimension five operators, one could introduce a discrete gauge symmetry that forbids the baryon number violating nonrenormalizable couplings. Since $B-L$ is the only anomaly free global symmetry in the standard model, we chose to impose a discrete subgroup of $B-L$. In models I and II the leptoquark has $B-L = 4/3$. The usual Z_2 , where the nontrivial transformation is $(-1)^{B-L}$, doesn't work, as the

operators \mathcal{O}_I , $\mathcal{O}_{II}^{(1)}$, and $\mathcal{O}_{II}^{(2)}$ are invariant under this transformation. However, we find that imposing a Z_3 discrete symmetry, with elements that are powers of $\exp[2\pi i(B - L)/3]$, forbids these dimension five operators and, thus, prevents the proton from decaying in this class of models. Note that gauging $B - L$ and spontaneously breaking the symmetry with a charge three scalar (at some high scale) leaves this unbroken discrete Z_3 gauge symmetry. It is not possible to use any discrete subgroup of $B - L$ to forbid proton decays in the models from Table 3.1 which exhibit proton decay at tree level since all the interactions conserve $B - L$.

Finally, we would like to comment on the relation between this work and that of [40], where renormalizable models that have additional scalars and have baryon number violation at tree level but not proton decay were enumerated and discussed. In these models none of the scalars were leptoquarks (they could rather be called diquarks or dileptons). However, if we permit higher dimension operators, then models 4 and 9 containing the scalar $X = (3, 1, 2/3)$ (which has renormalizable diquark couplings), have dimension five leptoquark-type couplings,

$$\mathcal{O}_{III} = \frac{1}{\Lambda} g^{ab} (\bar{Q}_L^{\alpha a} H) e_R^b X_\alpha . \quad (3.28)$$

This operator, combined with the renormalizable couplings of X to two quarks, gives proton decay with the rate estimated in Eq. (3.26). This observation restricts the parameter space of models 4 and 9 presented in [40] to the one in which either the color triplet scalar X is very heavy or its Yukawa couplings are small.

3.5 Conclusions

We have investigated the minimal set of renormalizable models in which a single scalar leptoquark is added to the standard model with the requirement that proton decay not be induced by scalar exchange. We have looked in detail at one particular model which gives an unusual top quark mass enhancement of the branching ratio of $\mu \rightarrow e\gamma$.

For this model, we have compared the $\mu \rightarrow e\gamma$ branching ratio to the $\mu \rightarrow e$ conversion rate in light of current constraints and future experiments. We find that the most stringent constraints on this model could come from the Mu2e experiment, and we have shown the potential limits both the MEG and Mu2e experiments could place on some of the couplings of the scalar leptoquark to the $\bar{Q}e$ and $L\bar{u}$ bilinears.

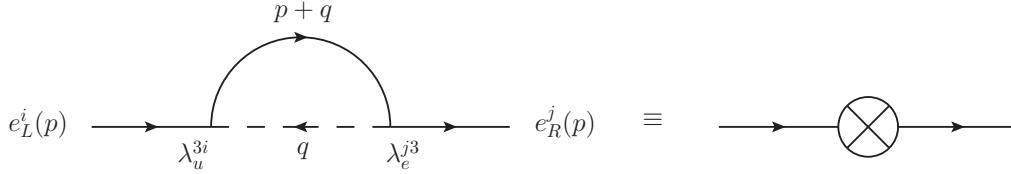
We have also shown the constraints on this model coming from the most recent limits on the electron EDM. Although the electron EDM also has the unusual enhancement from the top quark mass, the constraints are not so strong when compared with lepton flavor violating effects.

We have commented on the existence of nonrenormalizable operators in these minimal models which can give an unacceptably large proton decay rate for $m_V \lesssim 10\,000$ TeV, as well as provided a simple mechanism for avoiding them.

Appendix

3.A Calculation of $\mu \rightarrow e\gamma$

We will focus on the contribution to the $\mu \rightarrow e\gamma$ amplitude coming from terms proportional to $\lambda_u\lambda_e$. The other contributions are easily computed in a similar manner. We begin with the subdiagram,



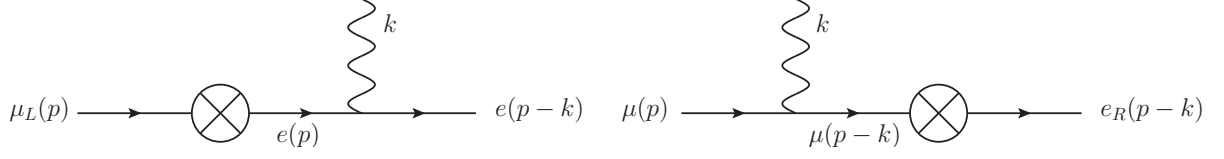
The corresponding amplitude is

$$\begin{aligned}
 i\mathcal{M} &= m_t \lambda_u^{3i} \lambda_e^{j3} \int \frac{d^4 q}{(2\pi)^4} P_R \frac{1}{[(p+q)^2 - m_t^2][q^2 - M_V^2]} \\
 &= m_t \lambda_u^{3i} \lambda_e^{j3} P_R A(p^2)
 \end{aligned} \tag{3.29}$$

Expanding $A(p^2)$ for small p^2 , we find $A(p^2) \simeq A(0) + p^2 A'(0)$ where

$$A'(0) = \frac{i}{16\pi^2 M_V^2} f\left(\frac{m_t^2}{M_V^2}\right), \quad f(x) = \frac{x^2 - 1 - 2x \ln x}{2(x-1)^3}. \tag{3.30}$$

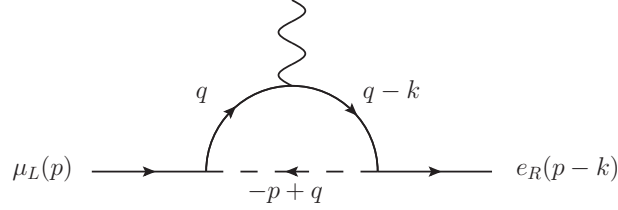
This subdiagram appears in the relevant diagrams,



We can write the amplitude coming from these two diagrams as

$$\begin{aligned}
i\mathcal{M} &= m_t \lambda_u^{3i} \lambda_e^{j3} \bar{e}(p-k) (-ie\gamma_\mu) i \frac{\not{p} + m_e}{m_\mu^2 - m_e^2} A(p^2) P_L \mu(p) \\
&\quad + \bar{e}(p-k) i \frac{\not{p} - \not{k} + m_\mu}{m_e^2 - m_\mu^2} A((p-k)^2) P_R (-ie\gamma_\mu) \mu(p) \\
&= m_t \lambda_u^{3i} \lambda_e^{j3} e m_\mu \frac{i}{16\pi^2 M_V^2} f\left(\frac{m_t^2}{M_V^2}\right) [\bar{e}(p-k) P_L \gamma_\mu \mu(p)] \quad (3.31)
\end{aligned}$$

The third diagram contributing to the $\mu \rightarrow e\gamma$ process involves a photon connected to the top quark in the loop,



giving an amplitude

$$\begin{aligned}
i\mathcal{M} &= -\frac{2}{3} m_t \lambda_u^{3i} \lambda_e^{j3} e \int \frac{d^4 q}{(2\pi)^4} \frac{\bar{e}_R(p-k) [(\not{q} - \not{k})\gamma_\mu + \gamma_\mu \not{q}] \mu_L(p)}{[(q-k)^2 - m_t^2] [q^2 - m_t^2] [(q-p)^2 - M_V^2]} \\
&= \frac{2}{3} m_t \lambda_u^{3i} \lambda_e^{j3} e \frac{i}{16\pi^2 M_V^2} \bar{e}_R(p-k) \left(k_\mu f_1(x) + p_\mu f_2(x) - (k_\mu + \frac{1}{2} [k, \gamma_\mu]) f_3(x) \right) \mu_L(p) \quad (3.32)
\end{aligned}$$

for $x = m_t^2/M_V^2$ where we've linearized the result with respect to external momenta and

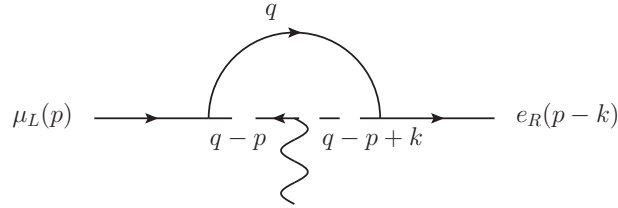
defined

$$f_1(x) = \frac{x^2 - 4x + 2 \ln x + 3}{2(x-1)^3} \quad (3.33)$$

$$f_2(x) = \frac{x^2 - 2x \ln x - 1}{(x-1)^3} \quad (3.34)$$

$$f_3(x) = \frac{x - \ln x - 1}{(x-1)^2}. \quad (3.35)$$

The final diagram to consider is the one with photon connected to the internal scalar line,



giving a contribution to the amplitude

$$\begin{aligned} i\mathcal{M} &= \bar{e}_R(p-k)(-i\lambda_u^{32})(-i\lambda_e^{13}) \int \frac{d^4q}{(2\pi)^4} i \frac{\not{q} + m_t}{q^2 - m_t^2} \mu_L(p) \\ &\quad \times \frac{i}{(q-p)^2 - M_V^2} (i\frac{5}{3}e) (2q^\mu - 2p^\mu + k^\mu) \frac{i}{(q-p+k)^2 - M_V^2} \\ &= -\frac{5}{3}m_t\lambda_u^{32}\lambda_e^{13} e \bar{e}_R(p-k)\mu_L(p) \\ &\quad \times \int \frac{d^4q}{(2\pi)^4} \frac{2q^\mu - 2p^\mu + k^\mu}{[(q-p+k)^2 - M_V^2][(q-p)^2 - M_V^2][q^2 - m_t^2]} \\ &= \frac{5}{3}m_t\lambda_u^{32}\lambda_e^{13} e \frac{i}{16\pi^2 M_V^2} \bar{e}_R(p-k) \left((2p_\mu - k_\mu)f_4(x) + (k_\mu - 2p_\mu)f_5(x) \right) \mu_L(p) \end{aligned} \quad (3.36)$$

where again we have linearized with respect to external momenta and defined

$$f_4(x) = \frac{2x^2 \ln x + (4-3x)x - 1}{2(x-1)^3} \quad (3.37)$$

$$f_5(x) = \frac{x \ln x - x + 1}{(x-1)^2}. \quad (3.38)$$

Finally, putting the amplitudes from all four of these diagrams together we find that all terms proportional to either p_μ or k_μ cancel out and we are left with just the terms proportional to $k^\nu \sigma_{\mu\nu}$. The total amplitude is

$$i\mathcal{M} = \frac{m_t e \lambda_u^{32} \lambda_e^{13}}{16\pi^2 M_V^2} \bar{e}_R(p-k) \sigma^{\mu\nu} k^\nu \mu_L(p) \times \frac{1}{2(x-1)^3} \left(x^2 - 1 - 2x \ln x + \frac{4}{3}(x-1)(x - \ln x - 1) \right). \quad (3.39)$$

The only other combination of couplings that will lead to an amplitude enhanced by the top quark mass is $\lambda_e^* \lambda_u^*$ and the calculation is nearly identical to the case we have just done.

Chapter 4

Supersymmetric Dark Matter Sectors

4.1 Introduction

The possibility to describe the properties of the cold dark matter in the universe using a candidate in various particle physics scenarios has been studied for a long time. For a review of different candidates see Ref. [47]. One of the most popular dark matter candidates is the lightest supersymmetric particle in SUSY theories. In this type of scenario typically one considers the lightest neutralino [48, 49, 50] or the gravitino [51] as dark matter candidates. Both candidates have been investigated in great detail by many experts in the field. Unfortunately, in these models one has a large number of free parameters and it is difficult to make unique predictions which can be tested in current or future dark matter experiments.

It is well-known that in order to guarantee the stability of the lightest neutralino in supersymmetric models the so-called R-parity symmetry is assumed. The case of the gravitino is different because its lifetime can be large enough even if R-parity is broken [51]. The possibility to understand the origin of R-parity conservation has been investigated by many groups. However, the simplest way to study this issue is to consider the $B - L$ extensions of the Minimal Supersymmetric Standard Model (MSSM) where after symmetry breaking one can obtain R-parity as a symmetry at the low-scale. See Refs. [52, 53, 68, 69, 70, 57, 58] for the study of this problem in some supersymmetric

scenarios and Refs. [59, 60, 61] for recent phenomenological studies of these models. Unfortunately, even if in these scenarios we can understand dynamically the origin of R-parity conservation it is difficult to make interesting predictions for dark matter experiments since we can have several dark matter candidates, the neutralinos or right-handed sneutrinos, and as in the MSSM there are many free parameters.

In this Letter we investigate the properties of a dark matter sector where supersymmetry is a good symmetry before the breaking of the gauge symmetry. In this context we do not need to impose a discrete symmetry to guarantee the stability of the dark matter candidate and even if R-parity is broken in the visible sector the dark matter candidate is stable. To study this idea of having a supersymmetric sector we consider a simple scenario where in the visible sector we have the minimal $B - L$ extension of the MSSM [67] and in the dark sector we have two chiral superfields with $B - L$ quantum numbers. Here the link between the visible and dark sector is defined by the $B - L$ gauge force which is broken in the visible sector by the vacuum expectation value (VEV) of the right-handed sneutrinos. We find that after the $B - L$ breaking a mass splitting is induced in the dark sector and the lightest field is the only possible candidate for the cold dark matter in the universe. In this model the dark matter candidate annihilates mainly into two sfermions when these channels are available. We investigate the different scenarios where we can achieve the observed dark matter relic density and the possible predictions for dark matter experiments. We find that the current bounds from the Xenon100 experiment set strong constraints on this type of models where the elastic dark matter nucleon cross section is through a neutral gauge boson.

This article is organized as follows: In Section 4.2, we define a simple scenario with a supersymmetric dark matter sector. In Section 4.3, we show the possible scenarios where one can achieve the relic density observed by the experiments. The constraints coming from the direct detection experiments are investigated in Section 4.4, while we summarize the main results in Section 4.5.

4.2 Supersymmetric Dark Sector

In general we can consider a simple extension of the standard model which is composed of a visible sector, a dark matter sector and the interactions between them. In this case the Lagrangian can be written as

$$\mathcal{L} = \mathcal{L}_{visible} + \mathcal{L}_{dark} + \mathcal{L}_{link}. \quad (4.1)$$

The visible sector here could be the Standard Model (SM) or any well-known extension of the SM. Since we are interested in the case where the dark sector is supersymmetric, one can have a model with broken SUSY in the visible sector, but SUSY still is a good symmetry in the dark matter sector. In order to achieve this type of scenario we can assume that supersymmetry breaking is mediated as in “gauge mediation”, where the messenger fields only have quantum numbers of the visible sector, and the soft terms induced by gravity are very small. Then, the SM singlet fields in the dark sector do not get large soft terms from gravity mediation. In this way, we can say that supersymmetry is a good symmetry in the dark sector.

In order to illustrate this idea we will use as visible sector the simplest $B - L$ extension of the MSSM [67] where one can understand the origin of R-parity violating interactions. The dark sector will be composed of the chiral superfields \hat{X} and $\hat{\bar{X}}$ with $B - L$ quantum numbers $\pm n_{BL}$. Then, the Lagrangian reads as

$$\mathcal{L}_{SDM} = \mathcal{L}_{B-L} + \mathcal{L}_{DM}, \quad (4.2)$$

where

$$\begin{aligned}
\mathcal{L}_{DM} = & \int d^2\theta d^2\bar{\theta} \hat{X}^\dagger e^{g_{BL} n_{BL} \hat{V}_{BL}} \hat{X} \\
& + \int d^2\theta d^2\bar{\theta} \hat{X}^\dagger e^{-g_{BL} n_{BL} \hat{V}_{BL}} \hat{X} \\
& + \left(\int d^2\theta \mu_X \hat{X} \hat{X} + \text{h.c.} \right), \tag{4.3}
\end{aligned}$$

and the superpotential of the minimal $B - L$ model is given by

$$\begin{aligned}
\mathcal{W}_{B-L} = & Y_u \hat{Q} \hat{H}_u \hat{u}^c + Y_d \hat{Q} \hat{H}_d \hat{d}^c + Y_e \hat{L} \hat{H}_d \hat{e}^c \\
& + Y_\nu \hat{L} \hat{H}_u \hat{\nu}^c + \mu \hat{H}_u \hat{H}_d. \tag{4.4}
\end{aligned}$$

See Refs. [67, 80] for the details of the minimal $B - L$ extension of the MSSM. It is important to mention that there is no need to add extra Higgses in the visible sector in order to break the $B - L$ gauge symmetry. In this case $B - L$ is broken by the VEV of the right-handed sneutrinos as studied in Refs. [67, 80]. We will show that once the right-handed sneutrino gets a VEV R-parity is spontaneously broken, but still the dark matter candidate is stable. Here we assume that the fields, X and \bar{X} , do not have interactions with the right-handed neutrinos, i.e., the couplings $(\hat{\nu}^c \hat{\nu}^c)^p \hat{X}^n$ are not present. This means that $2p - n n_{BL} \neq 0$, where n and p are integer numbers.

One of the most interesting consequences of having ‘‘exact’’ supersymmetry in the dark sector is that the scalar fields, X and \bar{X} , do not get a VEV in most of the cases. Using the Lagrangian above we can compute the scalar potential for the X and \bar{X} fields,

$$\begin{aligned}
V(X, \bar{X}) = & |\mu_X|^2 (|X|^2 + |\bar{X}|^2) \\
& + \frac{g_{BL}^2}{8} \left(\frac{v_R^2}{2} + n_{BL} (|X|^2 - |\bar{X}|^2) \right)^2. \tag{4.5}
\end{aligned}$$

Notice that here we have included the contribution to the $B - L$ D-term due to the VEV of right-handed sneutrinos, $\langle \tilde{\nu}^c \rangle = v_R/\sqrt{2}$, the field which breaks $B - L$ in the visible sector.

Then, one can see from the above equation that once $B - L$ is broken we induce a mass splitting between the scalar fields in the dark matter sector. The relevant scalar potential for our discussion is given by

$$V(v_X, v_{\bar{X}}) = \frac{1}{2}M_X^2 v_X^2 + \frac{1}{2}M_{\bar{X}}^2 v_{\bar{X}}^2 + \frac{g_{BL}^2 n_{BL}^2}{32} (v_X^2 - v_{\bar{X}}^2)^2, \quad (4.6)$$

where

$$M_X^2 = |\mu_X|^2 + \frac{g_{BL}^2}{8} n_{BL} v_R^2, \quad M_{\bar{X}}^2 = |\mu_X|^2 - \frac{g_{BL}^2}{8} n_{BL} v_R^2, \quad (4.7)$$

and we find the following minimization conditions:

$$\left(M_X^2 + \frac{g_{BL}^2}{8} n_{BL}^2 (v_X^2 - v_{\bar{X}}^2) \right) v_X = 0, \quad (4.8)$$

$$\left(M_{\bar{X}}^2 - \frac{g_{BL}^2}{8} n_{BL}^2 (v_X^2 - v_{\bar{X}}^2) \right) v_{\bar{X}} = 0. \quad (4.9)$$

Now, we can think about different scenarios:

- Case 1) We can have the trivial solutions, $v_X = v_{\bar{X}} = 0$, and the lightest field in the dark sector is stable.
- Case 2) $v_X \neq 0$ and $v_{\bar{X}} \neq 0$: Using the Eq.(4.8), and Eq.(4.9) we can show that in this case there is a solution only when $\mu_X = 0$. However, in this case the fermion partners \tilde{X} and $\tilde{\bar{X}}$ are massless.
- Case 3) $v_X = 0$ and $v_{\bar{X}} \neq 0$: In this case we can have the solution

$$v_{\bar{X}}^2 = -\frac{8M_{\bar{X}}^2}{g_{BL}^2 n_{BL}^2}. \quad (4.10)$$

if $M_{\bar{X}}^2 < 0$.

- Case 4) $v_X \neq 0$ and $v_{\bar{X}} = 0$: There is no solution in this case.

Then, in general we can say that the scalar fields do not get a VEV even if they have a mass splitting due to the $B - L$ D-term and when $M_{\bar{X}}^2 > 0$. This is an important result

which guarantees the stability of the lightest field in the dark sector and we do not need to impose any extra discrete symmetry. Notice that in this analysis we have neglected the contribution from the kinetic mixing between hypercharge and B-L, which does not change our conclusion.

In order to understand the existence of a dark matter candidate let us study the spectrum in the dark matter sector. In Eq. (4.7) we have the masses for the scalar fields, while the mass of the fermionic candidates is

$$\mathcal{M}_{\tilde{X}_1} = \mathcal{M}_{\tilde{X}_2} = \mu_X. \quad (4.11)$$

Therefore, the lightest field in the dark sector is the scalar field \bar{X} . Here we are using the convention where n_{BL} is positive. Now, are these fields stable at cosmological scales?

The field X can decay into its superpartner \tilde{X} and SM fermions because R-parity is broken in the visible sector. In the case of $\tilde{\bar{X}}$ and \tilde{X} we have a similar situation, they can decay to \bar{X} and SM fermions as well. Therefore, only the lightest field in the dark sector, \bar{X} , can be stable even if R-parity is broken in the visible sector. This is an interesting result which is a consequence of having “exact” supersymmetry in the dark matter sector before $B - L$ is broken in the visible sector. Before we finish this section we would like to stress the existence of the relation between the masses of all fields in the dark sector:

$$M_X^2 = M_{\tilde{X}}^2 + \frac{1}{2}n_{BL}M_{Z_{BL}}^2 = M_{\bar{X}}^2 + n_{BL}M_{Z_{BL}}^2, \quad (4.12)$$

where the mass of the $B - L$ neutral gauge boson is given by $M_{Z_{BL}} = g_{BL}v_R/2$. Notice that the supertrace mass formula, $\text{Str } M^2 = 0$, is valid here since we have the same splitting for the scalar components, but with different signs. Here we neglect possible Planck scale suppressed operators due to gravity effects.

4.3 Dark Matter Relic Density

The $B - L$ D-term defines how the dark matter candidate annihilates into two sfermions when these channels are available. Here we will focus on the scenarios where the dark matter candidate is always heavier than a least one sfermion in the MSSM. In the case when the mass of \bar{X} is below $M_{Z_{BL}}/2$ the main annihilation channels are in fact those with two sfermions:

$$\bar{X}\bar{X}^\dagger \rightarrow \tilde{f}_i \tilde{f}_i^\dagger, \quad (4.13)$$

and the annihilation cross section in the non-relativistic limit is given by

$$\sigma \left(\bar{X}\bar{X}^\dagger \rightarrow \tilde{f}_i \tilde{f}_i^\dagger \right) v = \frac{1}{64\pi} \frac{1}{M_{\bar{X}}^2} \sqrt{1 - \frac{M_{\tilde{f}_i}^2}{M_{\bar{X}}^2} |\lambda|^2} \left| 1 + \frac{M_{Z_{BL}}^2}{4M_{\bar{X}}^2 - M_{\tilde{\nu}^c}^2} \right|^2 \quad (4.14)$$

Here $M_{\tilde{\nu}^c} = M_{Z_{BL}}$ and $\lambda = g_{BL}^2 n_{BL}/4$ for sleptons. Now, we can compute the approximate freeze-out temperature $x_f = M_{\bar{X}}/T_f$. Writing the thermally averaged annihilation cross section as $\langle \sigma v \rangle = \sigma_0 (T/M_X)^n$, then the freeze-out temperature is given by

$$\begin{aligned} x_f &= \ln \left[0.038(n+1) \left(\frac{g}{\sqrt{g_*}} \right) M_{Pl} M_{\bar{X}} \sigma_0 \right] \\ &\quad - \left(n + \frac{1}{2} \right) \ln \left[\ln \left[0.038(n+1) \left(\frac{g}{\sqrt{g_*}} \right) M_{Pl} M_{\bar{X}} \sigma_0 \right] \right], \end{aligned} \quad (4.15)$$

where M_{Pl} is the Planck mass, g is the number of internal degrees of freedom and g_* is the effective number of relativistic degrees of freedom evaluated around the freeze-out temperature. As is well-known, the present day energy density of the relic dark matter particles \bar{X} is given by

$$\Omega_X h^2 = \frac{1.07 \times 10^9}{\text{GeV}} \left(\frac{(n+1)x_f^{n+1}}{\sqrt{g_*} \sigma_0 M_{Pl}} \right), \quad (4.16)$$

where we have used the fact that $g_{*,S}(T) = g_*(T)$ in our case (all particle species have a common temperature). We will use the present day dark matter energy density to be $\Omega_{DM}h^2 = 0.112 \pm 0.006$ [64] for our numerical study and in our case $n = 0$.

It is important to mention that in this model we have the following free parameters:

$$M_{Z_{BL}}, g_{BL}, M_{\bar{X}}, n_{BL}, \quad (4.17)$$

together with MSSM parameters $M_{\tilde{f}_i}$, and $\tan \beta$. Our results are not very sensitive to the values of $\tan \beta$ since the annihilation cross section in our study is basically independent of this parameter. In order to illustrate our main idea we will show the numerical results in simplified models where the dark matter candidate can annihilate into two MSSM sleptons when these channels are available. When the dark matter mass is below the slepton mass one can have the annihilation into two SM fermions at the one-loop level. In this Letter we will focus on the simplest possibility which corresponds to the case when \bar{X} is always heavier than the sleptons in the MSSM and the squarks are much heavier. Before we do the numerical analysis it is important to understand the spectrum of sfermions in this theory. This aspect of the theory has been studied in Ref. [80]. Here we will assume for simplicity that the lightest sfermions are the sleptons, and their masses are given by

$$M_{\tilde{\nu}_i}^2 = M_{\tilde{L}_i}^2 + \frac{1}{2}M_Z^2 \cos 2\beta - \frac{1}{2}M_{Z_{BL}}^2, \quad (4.18)$$

$$M_{\tilde{e}_i}^2 = M_{\tilde{L}_i}^2 + M_{e_i}^2 - \left(\frac{1}{2} - \sin^2 \theta_W^2 \right) M_Z^2 \cos 2\beta - \frac{1}{2}M_{Z_{BL}}^2. \quad (4.19)$$

Notice that the rest of the fields with positive $B - L$ are heavier due to the positive contribution from the $B - L$ D-term. In Fig. 4.1 we show the allowed values for the gauge coupling g_{BL} and DM mass $M_{\bar{X}}$ when $\tan \beta = 6$, $M_{Z_{BL}}/g_{BL} = 4$ TeV, $M_{\tilde{e}} = 200$ GeV and $n_{BL} = 1/3$. Here we assume a simplified model where the annihilation is only possible to one family of sleptons. Notice that for this type of scenario the gauge coupling has to be changed between 10^{-1} and $10^{-0.4}$, in order to achieve the relic density consistent

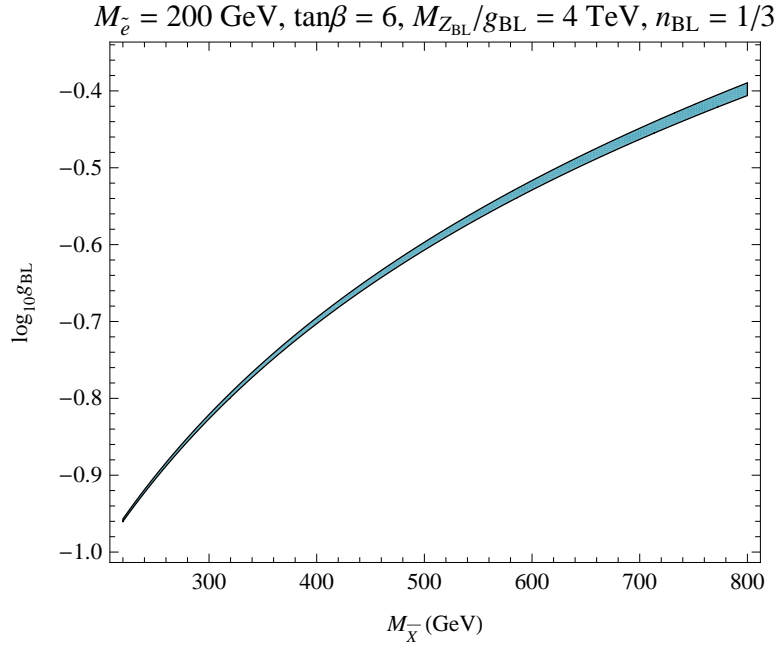


Figure 4.1: Allowed values for the gauge coupling g_{BL} and $M_{\tilde{X}}$ when $\tan\beta = 6$, $M_{Z_{BL}}/g_{BL} = 4 \text{ TeV}$, $M_{\tilde{e}} = 200 \text{ GeV}$ and $n_{BL} = 1/3$. Here we assume the annihilation to only one family of sleptons. The black lines produce $\Omega h^2 = 0.112$ while the blue region represents $\Omega h^2 \leq 0.112$.

with cosmological observations. As we will discuss later, this type of scenario is allowed by the constraints coming from direct detection experiments, which we discuss in detail in the next section.

In order to have a better idea of how to achieve the right relic density we show in Fig. 4.2 the values for the relic density when changing the dark matter mass $M_{\tilde{X}}$, when $\tan\beta = 6$, $n_{BL} = 1/3$, and $M_{Z_{BL}}/g_{BL} = 4 \text{ TeV}$. Here the blue dots correspond to the solutions for $g_{BL} = 0.1 \div 0.2$, the green dots are for $g_{BL} = 0.2 \div 0.3$, the orange dots are for $g_{BL} = 0.3 \div 0.4$, and the red dots are for $g_{BL} = 0.4 \div 0.5$. We also scan over the slepton mass between 100 GeV and the dark matter mass. Notice that we find many solutions which are consistent with relic density bounds when the gauge coupling is between 0.3 and 0.5.

It is easy to understand the results presented in Fig. 4.1 and Fig. 4.2. When the gauge coupling is small or we increase the dark matter mass we suppress the annihilation cross section, we can achieve the relic density allowed by the experiments. The only way to

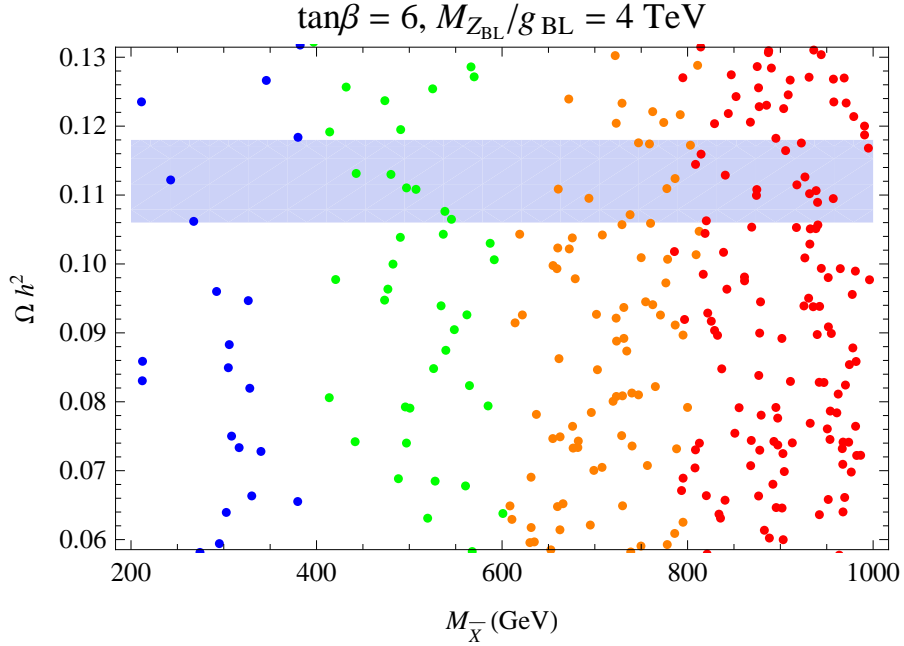


Figure 4.2: Values for the relic density vs the dark matter mass $M_{\bar{X}}$, when $\tan\beta = 6$, $n_{BL} = 1/3$, and $M_{Z_{BL}}/g_{BL} = 4 \text{ TeV}$. Here the blue dots correspond to the solutions for $g_{BL} = 0.1 \div 0.2$, the green dots are for $g_{BL} = 0.2 \div 0.3$, the orange dots are for $g_{BL} = 0.3 \div 0.4$, and the red dots are for $g_{BL} = 0.4 \div 0.5$. The slepton mass changes between 100 GeV and the dark matter mass.

achieve solutions when the gauge coupling is close to one is to suppress the phase space choosing a small splitting between the slepton mass and the dark matter mass. Notice that the annihilation through the Z_{BL} is suppressed in these scenarios because the $B - L$ gauge boson is very heavy and the cross section is p-wave suppressed. Also we can have other annihilation channels into two quarks at one-loop level, but these are also suppressed by the squark masses.

4.4 Predictions for DM Direct Detection

The couplings of the Z_{BL} to quarks and the dark matter candidate, \bar{X} , can lead to a potentially sizeable spin-independent elastic scattering cross section between dark matter and

nuclei. The cross section in this case is given by

$$\sigma^{\text{SI}} = \frac{M_{\bar{X}}^2 m_N^2}{\pi(M_{\bar{X}} + m_N)^2} \left[Z f_p + (A - Z) f_n \right]^2, \quad (4.20)$$

where A and Z are the atomic mass and atomic number of the target nucleus and $f_{(p,n)}$ are the effective couplings to protons and neutrons:

$$f_p = \frac{g_{\bar{X}\bar{X}Z_{BL}}(2g_{uuZ_{BL}} + g_{ddZ_{BL}})}{M_{Z_{BL}}^2}, \quad (4.21)$$

$$f_n = \frac{g_{\bar{X}\bar{X}Z_{BL}}(g_{uuZ_{BL}} + 2g_{ddZ_{BL}})}{M_{Z_{BL}}^2}. \quad (4.22)$$

Here, we have used $g_{\bar{X}\bar{X}Z_{BL}}$ and $g_{qqZ_{BL}}$ to denote the effective coupling strengths of the respective vertices. For any quark we have $g_{qqZ_{BL}} = g_{BL}/6$ and $g_{\bar{X}\bar{X}Z_{BL}} = n_{BL}g_{BL}/2$. Now, using the relations above we can write the dark matter nucleon cross section as

$$\sigma_{\bar{X}n}^{\text{SI}} (\text{cm}^2) = (1.2 \times 10^{-40} \text{ cm}^2) \times g_{BL}^4 n_{BL}^2 \times \left(\frac{500 \text{ GeV}}{M_{Z_{BL}}} \right)^4 \times \left(\frac{\mu}{1 \text{ GeV}} \right)^2, \quad (4.23)$$

where $\mu = M_{\bar{X}}m_n/(M_{\bar{X}} + m_n)$, and m_n is the nucleon mass. It is well-known that the dark matter spin-independent elastic cross sections are tightly constrained by the Xenon100 experimental results [65]. In Fig. 4.3 we show the numerical values for the elastic DM-nucleon cross section as a function of the dark matter mass $M_{\bar{X}}$. Here we use different values for the ratio $M_{Z_{BL}}/(g_{BL}\sqrt{n_{BL}})$ and show the bounds from Xenon10 [66] and Xenon100 [65] experiments. The best limits on our model come from Xenon100, which for $M_{\bar{X}} \gtrsim 30 \text{ GeV}$ rules out most of the region $M_{Z_{BL}}/(g_{BL}\sqrt{n_{BL}}) < 6 \text{ TeV}$. On the other hand, ratios $M_{Z_{BL}}/(g_{BL}\sqrt{n_{BL}})$ as low as 1 TeV are allowed for light dark matter masses, $M_{\bar{X}} \lesssim 8 \text{ GeV}$. It is important to mention that the collider bound on the $B - L$ gauge boson is about $M_{Z_{BL}}/g_{BL} > 3 \text{ TeV}$. Then, we can say that the dark matter experiment Xenon100 sets a strong bound on the gauge boson mass if n_{BL} is not very small.

In Fig. 4.4 we show the correlation between the values for the spin-independent cross

Spin-independent cross section

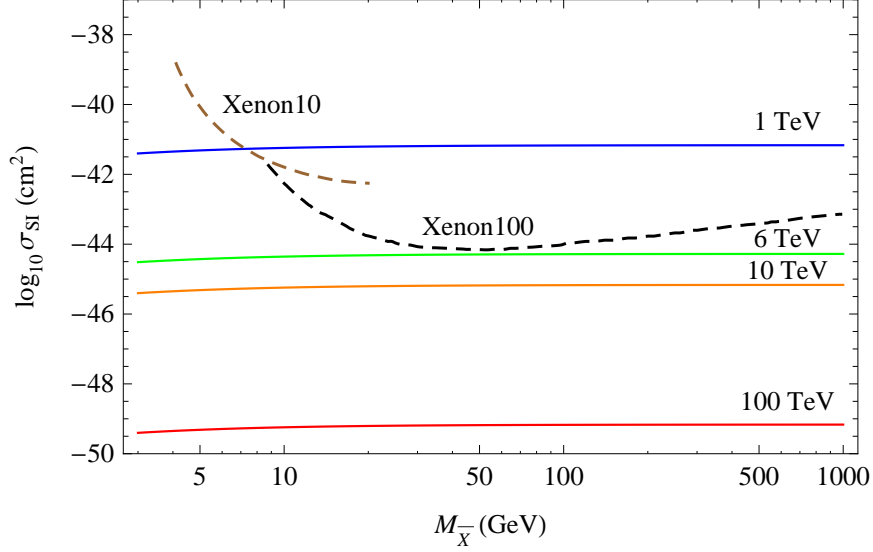


Figure 4.3: Values for the spin-independent elastic DM-nucleon cross section for a few different ratios $M_{Z_{BL}}/(g_{BL}\sqrt{n_{BL}})$: 1 TeV (blue), 6 TeV (green), 10 TeV (orange), and 100 TeV (red). The black dashed line is the exclusion limit from Xenon100 and the brown dashed line is the exclusion limit from Xenon10. Note that the 6 TeV line in this plot is consistent with our earlier choice of $M_{Z_{BL}}/g_{BL} = 4$ TeV when $n_{BL} = 1/3$.

section and the dark matter relic density when $M_{\tilde{e}} = 100$ GeV, $\tan \beta = 6$, $n_{BL} = 1/3$, $0.1 \text{ TeV} \leq M_{Z_{BL}} \leq 10 \text{ TeV}$, and $0.1 \leq g_{BL} \leq 1$, for different values of the dark matter mass. Then, in this way we can see that there are not many allowed solutions by the relic density constraints assuming the mentioned values of the free parameters. Since the range of the parameter space is quite representative we can say that it is not easy to find solutions in agreement with the experiments. If we think about the testability of this model for dark matter one can imagine a very optimistic scenario where we can know the parameters $M_{Z_{BL}}$, g_{BL} , $M_{\tilde{e}}$, and $\tan \beta$ from the Large Hadron Collider or future collider experiments. Then, we could get the rest of the parameters n_{BL} and the dark matter mass $M_{\tilde{X}}$ using the constraints from relic density and direct detection experiments. For example, suppose that in a dark matter experiment such as Xenon100 you find a signal which corresponds to a cross section of 10^{-45} cm^2 . If the collider experiments measure say, $g_{BL} = 0.3$, $\tan \beta = 6$, $M_{Z_{BL}} = 2$ TeV and $M_{\tilde{e}} = 200$ GeV and we require $\Omega h^2 \leq 0.112$, this corresponds

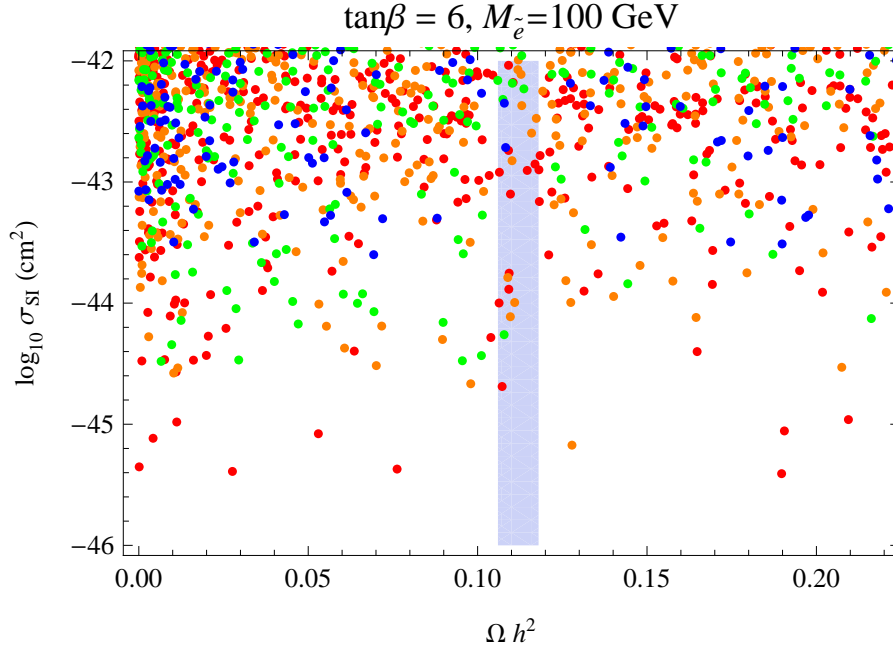


Figure 4.4: Values for the cross section allowed by the relic density constraints when the slepton mass is 100 GeV, $\tan\beta = 6$, $n_{BL} = 1/3$, $0.1 \text{ TeV} \leq M_{Z_{BL}} \leq 10 \text{ TeV}$, and $0.1 \leq g_{BL} \leq 1$. Blue, green, orange, and red dots correspond to $M_{\tilde{X}} = 120, 200, 300,$ and 400 GeV , respectively.

to $n_{BL} = 0.54$ and $986 \text{ GeV} \leq M_{\tilde{X}} \leq 1014 \text{ GeV}$. The bounds of this inequality achieve $\Omega h^2 = 0.112$. In this way we could think about the testability of this scenario.

4.5 Conclusions

In this Letter we have investigated a simple scenario for the cold dark matter in the universe where the sector responsible for dark matter has “exact” supersymmetry before symmetry breaking. In order to achieve this type of scenario we assume that supersymmetry breaking is mediated as in “gauge mediation”, where the messenger fields only have quantum numbers of the visible sector, and the soft terms induced by gravity are very small. The SM singlet fields in the dark sector do not get large soft terms from gravity mediation and we can say that supersymmetry is a good symmetry in the dark sector.

In order to illustrate our idea we consider the case where in the visible sector we have

the simplest $B - L$ extension of the minimal supersymmetric standard model while the dark sector is composed of two chiral superfields with $B - L$ quantum numbers. We have found that in this case the dark matter candidate is the lightest scalar field in the dark sector and the $B - L$ D-term induces a mass splitting after the symmetry is broken.

We noticed that the dark matter candidate is stable even if R-parity is spontaneously broken in the visible sector. Since the link between the visible and dark sectors is through the $B - L$ gauge force, the dark matter annihilates mainly into two sfermions when these channels are available. We have shown the allowed parameter space by the relic density and direct detection experiments in simplified scenarios where the annihilation is mainly into two sleptons. In the case when the dark matter candidate is below 100 GeV, the DM annihilation is mainly into two fermions at the one-loop level where inside the loops you have the sfermions and gauginos. The details of the scenario for light dark matter and the annihilation into photons will be investigated in a future publication.

Chapter 5

B and L at the SUSY Scale, Dark Matter and R-parity Violation

5.1 Introduction

The Minimal Supersymmetric Standard Model (MSSM) is considered one of the most appealing candidates for physics beyond the Standard Model. While the recent results from the Large Hadron Collider (LHC) have set serious constraints on the masses of the supersymmetric particles, if one suspects that new physics exists at an LHC accessible scale, an MSSM-like theory still highly recommends itself as a candidate theory.

Despite its various appealing properties, the MSSM poses a challenge for proton stability. This is because it introduces two separate sets of operators which induce proton decay: tree-level terms, which separately violate baryon and lepton number, and non-renormalizable terms which individually violate both baryon and lepton number. The first of these are

$$\hat{L}\hat{H}_u, \hat{L}\hat{L}\hat{e}^c, \hat{Q}\hat{L}\hat{d}^c, \text{ and } \hat{u}^c\hat{d}^c\hat{d}^c,$$

where the first three operators violate lepton number and the last baryon number. Any combination of the first three operators with the last one leads to rapid proton decay. Their absence is typically explained by invoking R-parity, an *ad hoc* discrete symmetry defined as $R = (-1)^{3(B-L)+2S}$, which forbids all of these terms. However, the fate of such operators

is most simply divined from models of gauged $B - L$. The most minimal of such models lead to lepton number violating R-parity violation (and therefore no tree-level proton decay) [67], but R-parity conserving models are also possible [68, 69, 70]. Regardless of the type of $B - L$ model, the second type of proton decay inducing operators exist. These are non-renormalizable operators which conserve $B - L$ but violate B and L separately, *e.g.*,

$$\hat{Q}\hat{Q}\hat{Q}\hat{L}/\Lambda, \text{ and } \hat{u}^c\hat{u}^c\hat{d}^c\hat{e}^c/\Lambda.$$

Despite the suppression in these terms due to the scale of new physics, the bounds on proton decay are strong enough to motivate a mechanism for suppressing them. See [71] for a review of proton decay.

Recently, a simple theory for the spontaneous breaking of local baryon and lepton numbers has been proposed in Ref. [72]. In this context one can define an anomaly free theory using fermionic leptoquarks which have both baryon and lepton number charges. Furthermore, even after symmetry breaking, the lightest leptoquark is stable due to a remnant Z_2 symmetry and can therefore be a dark matter candidate. See also Refs. [73, 74, 75] for similar studies. This idea can be applied in the context of supersymmetric theories to establish not only the origin of the R-parity violating terms, as in the $B - L$ models, but also determine the fate of the non-renormalizable terms which violate B and L separately.

In this paper we investigate an extension of the MSSM where the local baryonic and leptonic symmetries are spontaneously broken at the supersymmetry scale. We find that the minimal model predicts that R-parity must be spontaneously broken in the MSSM sector (leading only to lepton number violation). Despite the breaking of R-parity, the remnant Z_2 symmetry from the breaking of the baryonic and leptonic symmetries ensures that the lightest leptoquark is stable and may be a candidate for the cold dark matter of the universe. We investigate the spectrum of the theory and the predictions for dark matter direct detection. This article is organized as follows: In Section 5.2 we discuss the model with local B and L symmetries, in Section 5.3 we discuss the possible dark matter candidates and the predictions for dark matter experiments. Finally, we summarize our results in Section 5.4.

5.2 Spontaneous Breaking of B and L

In order to define a theory for local baryon and lepton numbers we use the gauge group,

$$SU(3)_C \otimes SU(2)_L \otimes U(1)_Y \otimes U(1)_B \otimes U(1)_L .$$

An anomaly free theory can be achieved by adding the following new leptoquark fields with B and L numbers [72]:

$$\begin{aligned} \hat{\Psi} &\sim (1, 2, -1/2, B_1, L_1) , & \hat{\Psi}^c &\sim (1, 2, 1/2, B_2, L_2) , \\ \hat{\eta}^c &\sim (1, 1, 1, -B_1, -L_1) , & \hat{\eta} &\sim (1, 1, -1, -B_2, -L_2) , \\ \hat{X}^c &\sim (1, 1, 0, -B_1, -L_1) , & \text{and } \hat{X} &\sim (1, 1, 0, -B_2, -L_2) . \end{aligned}$$

Notice that these fields are vector-like with respect to the SM transformations. The anomalies can be cancelled for any values of B_i and L_i ($i = 1, 2$) which satisfy the conditions

$$B_1 + B_2 = -3 , \text{ and } L_1 + L_2 = -3 . \quad (5.1)$$

In order to generate masses for the new fields and for symmetry breaking we need the chiral superfields,

$$\hat{S}_1 \sim (1, 1, 0, 3, 3) , \text{ and } \hat{S}_2 \sim (1, 1, 0, -3, -3) .$$

Therefore, the superpotential of this theory is given by

$$\mathcal{W}_{BL} = \mathcal{W}_{\text{RpC}} + \mathcal{W}_{\text{LB}} , \quad (5.2)$$

where

$$\begin{aligned}\mathcal{W}_{\text{RpC}} &= Y_u \hat{Q} \hat{H}_u \hat{u}^c + Y_d \hat{Q} \hat{H}_d \hat{d}^c + Y_e \hat{L} \hat{H}_d \hat{e}^c \\ &+ Y_\nu \hat{L} \hat{H}_u \hat{\nu}^c + \mu \hat{H}_u \hat{H}_d,\end{aligned}\tag{5.3}$$

contains the R-parity conserving terms present in the MSSM (plus a Yukawa coupling for the neutrinos, Y_ν), and

$$\begin{aligned}\mathcal{W}_{\text{LB}} &= Y_1 \hat{\Psi} \hat{H}_d \hat{\eta}^c + Y_2 \hat{\Psi} \hat{H}_u \hat{X}^c + Y_3 \hat{\Psi}^c \hat{H}_u \hat{\eta} + Y_4 \hat{\Psi}^c \hat{H}_d \hat{X} \\ &+ \lambda_1 \hat{\Psi} \hat{\Psi}^c \hat{S}_1 + \lambda_2 \hat{\eta} \hat{\eta}^c \hat{S}_2 + \lambda_3 \hat{X} \hat{X}^c \hat{S}_2 + \mu_{BL} \hat{S}_1 \hat{S}_2,\end{aligned}\tag{5.4}$$

is the superpotential of the leptoquark sector needed for anomaly cancellation. Of course, because of the conservation of B and L , both the R-parity violating terms and the non-renormalizable terms leading to proton decay are forbidden. Notice that when $B_1 = B_2$ and $L_1 = L_2$ we can have Majorana masses for the \hat{X} and \hat{X}^c , but we stick to the general case where the quantum numbers are different.

An interesting consequence of the leptoquark sector is the presence of a Z_2 symmetry once S_1 and S_2 acquire a VEV. Under this symmetry, all leptoquarks are odd: $\Psi \rightarrow -\Psi$, $\Psi^c \rightarrow -\Psi^c$, $\eta \rightarrow -\eta$, $\eta^c \rightarrow -\eta^c$, $X \rightarrow -X$ and $X^c \rightarrow -X^c$. The consequence of this is that the lightest leptoquark is stable (must be neutral) and therefore a dark matter candidate.

5.2.1 Symmetry Breaking and Gauge Boson Masses

Symmetry breaking in the baryon and lepton number sector proceeds through the following scalar potential:

$$\begin{aligned}
V = & (M_1^2 + |\mu_{BL}|^2) |S_1|^2 + (M_2^2 + |\mu_{BL}|^2) |S_2|^2 \\
& + M_{\tilde{\nu}^c}^2 |\tilde{\nu}^c|^2 + \frac{9}{2} g_B^2 (|S_1|^2 - |S_2|^2)^2 \\
& + \frac{1}{2} g_L^2 (3|S_1|^2 - 3|S_2|^2 - |\tilde{\nu}^c|^2)^2 \\
& - (b_{BL} S_1 S_2 + \text{h.c.}), \tag{5.5}
\end{aligned}$$

where M_1 , M_2 and $M_{\tilde{\nu}^c}$ are the soft terms for the scalar fields S_1 , S_2 and $\tilde{\nu}^c$, respectively. Here b_{BL} is the bilinear term between S_1 and S_2 and we define the vacuum expectation values (VEVs) as

$$\sqrt{2} S_1 = v_1 + h_1 + i a_1, \tag{5.6}$$

$$\sqrt{2} S_2 = v_2 + h_2 + i a_2, \tag{5.7}$$

$$\sqrt{2} \tilde{\nu}^c = v_R + h_R + i a_R. \tag{5.8}$$

The squared mass matrix for the new gauge bosons can be written as

$$\mathcal{M}_{Z'}^2 = 9 \begin{pmatrix} g_B^2 (v_1^2 + v_2^2) & g_B g_L (v_1^2 + v_2^2) \\ g_B g_L (v_1^2 + v_2^2) & g_L^2 (v_1^2 + v_2^2) + \frac{1}{9} g_L^2 v_R^2 \end{pmatrix}, \tag{5.9}$$

which has a zero determinant if $v_R = 0$; note that this cannot be modified even in the case where $\langle X \rangle \neq 0$. This is a consequence of the fact that when S_1 and S_2 acquire VEVs the symmetry group $U(1)_B \otimes U(1)_L$ is broken to $U(1)_{B-L}$. The $B - L$ symmetry can only be broken by the VEV of the right-handed sneutrino as in Ref. [67]. Therefore, we conclude that

R-parity must be spontaneously broken in this theory !

However, it is only lepton number violating R-parity violation and therefore the proton remains safe.

The minimization conditions read as

$$0 = (M_1^2 + |\mu_{BL}|^2) - b_{BL} \frac{v_2}{v_1} + \frac{9}{2} g_B^2 (v_1^2 - v_2^2) + \frac{3}{2} g_L^2 (3v_1^2 - 3v_2^2 - v_R^2), \quad (5.10)$$

$$0 = (M_2^2 + |\mu_{BL}|^2) - b_{BL} \frac{v_1}{v_2} - \frac{9}{2} g_B^2 (v_1^2 - v_2^2) - \frac{3}{2} g_L^2 (3v_1^2 - 3v_2^2 - v_R^2), \quad (5.11)$$

$$0 = M_{\tilde{\nu}^c}^2 - \frac{1}{2} g_L^2 (3v_1^2 - 3v_2^2 - v_R^2), \quad (5.12)$$

and can be reformulated as,

$$v_R^2 = \frac{2}{g_L^2} \left[-M_{\tilde{\nu}^c}^2 + \frac{3}{2} g_L^2 (v_1^2 - v_2^2) \right], \quad (5.13)$$

$$\sin(2\gamma) = \frac{2b_{BL}}{M_1^2 + M_2^2 + 2|\mu_{BL}|^2}, \quad (5.14)$$

where we have defined

$$\tan \gamma = \frac{v_2}{v_1}. \quad (5.15)$$

One can easily prove that there is no symmetry breaking in the SUSY limit. Therefore, the B and L breaking scales are determined by the SUSY scale. In order to have a potential bounded from below we must satisfy the condition,

$$2b_{BL} < M_1^2 + M_2^2 + 2|\mu_{BL}|^2, \quad (5.16)$$

and in order to break the symmetry we need the condition

$$b_{BL}^2 > \left(M_1^2 + |\mu_{BL}|^2 - \frac{3}{2} g_L^2 v_R^2 \right) \left(M_2^2 + |\mu_{BL}|^2 + \frac{3}{2} g_L^2 v_R^2 \right). \quad (5.17)$$

The mixing angle between Z_1 and Z_2 is defined by

$$\begin{pmatrix} Z_B \\ Z_L \end{pmatrix} = \begin{pmatrix} \cos \theta_{BL} & \sin \theta_{BL} \\ -\sin \theta_{BL} & \cos \theta_{BL} \end{pmatrix} \begin{pmatrix} Z_1 \\ Z_2 \end{pmatrix}, \quad (5.18)$$

where $M_{Z_1} < M_{Z_2}$. The eigenvalues for the new neutral gauge bosons are

$$M_{Z_{1,2}}^2 = \frac{1}{2} \left(M_{Z_L}^2 + M_{Z_B}^2 \pm \sqrt{\Delta_{BL}^2} \right), \quad (5.19)$$

where

$$\Delta_{BL}^2 = (M_{Z_L}^2 - M_{Z_B}^2)^2 + 4g_L^2 M_{Z_B}^4 / g_B^2, \quad (5.20)$$

$$M_{Z_B}^2 \equiv 9g_B^2(v_1^2 + v_2^2), \quad (5.21)$$

$$M_{Z_L}^2 \equiv 9g_L^2 \left(v_1^2 + v_2^2 + \frac{1}{9} v_R^2 \right), \quad (5.22)$$

and the mixing angle is given by

$$\sin(2\theta_{BL}) = \frac{2g_B g_L (v_1^2 + v_2^2)}{M_{Z_2}^2 - M_{Z_1}^2}. \quad (5.23)$$

Note that this produces a Z_1 lighter than Z_2 only for $M_{Z_B} < M_{Z_L}$. For the opposite case we take $\theta_{BL} \rightarrow -\theta_{BL}$ and $Z_1 \leftrightarrow Z_2$. In the limit $v_R^2 \gg v_1^2 + v_2^2$ the eigenvalues are

$$M_{Z_1} \sim 9g_B^2 (v_1^2 + v_2^2) (1 - 9\epsilon), \quad (5.24)$$

$$M_{Z_2} \sim g_L^2 v_R^2 (1 + 9\epsilon), \quad (5.25)$$

where $\epsilon \equiv (v_1^2 + v_2^2)/v_R^2$ and the mass eigenstates are,

$$Z_1 = \left(1 - \frac{81}{2} \frac{g_B^2}{g_L^2} \epsilon^2\right) Z_B - 9 \frac{g_B}{g_L} \epsilon Z_L, \quad (5.26)$$

$$Z_2 = 9 \frac{g_B}{g_L} \epsilon Z_B + \left(1 - \frac{81}{2} \frac{g_B^2}{g_L^2} \epsilon^2\right) Z_L. \quad (5.27)$$

This is an interesting limit since the lighter Z_1 eigenstate is predominately Z_B -like and therefore has lower collider bounds [77, 78] compared to a Z' that significantly couples to leptons [79].

Finally, we note that when baryon and lepton numbers are broken at the SUSY scale, one expects operators mediating proton decay. However, in this theory, the proton is stable because baryon number is broken by three units. The least suppressed non-renormalizable terms which generate baryon and lepton number violating interactions occur at dimension 14, *e.g.*,

$$\mathcal{W}_{14} = \frac{1}{\Lambda^{10}} \left[c_1 \hat{S}_1 (\hat{u}^c \hat{u}^c \hat{d}^c \hat{e}^c)^3 + c_2 \hat{S}_1 (\hat{u}^c \hat{d}^c \hat{d}^c \hat{\nu}^c)^3 + c_3 \hat{S}_2 (\hat{Q} \hat{Q} \hat{Q} \hat{L})^3 \right]. \quad (5.28)$$

Due to this large suppression, there is no need to assume a large scale to be in agreement with experiments.

5.2.2 Spontaneous R-parity Violation

As we saw earlier, in order to avoid a long range $B - L$ force, the sneutrino must acquire a VEV. The consequences of this are very similar to those in the minimal supersymmetric $B - L$ model [67] and we briefly review them here.

The first and most obvious of these consequences is that R-parity is spontaneously broken. This induces a mixing between SUSY and non-SUSY fields with the same quantum numbers: neutralinos with neutrinos, charginos with charged leptons, sneutrinos with neutral Higgs and charged sleptons with charged Higgs. Typically, the most important of these mixings proceeds through the neutrino Yukawa coupling in the superpotential once the

right-handed sneutrino acquires a VEV, and one obtains

$$W \supset \frac{1}{\sqrt{2}} Y_\nu v_{R\ell} \tilde{H}_u, \quad (5.29)$$

which is the so-called bilinear R-parity violating term usually referred to as μ' . This term also induces a VEV for the left-handed sneutrino which leads to various mixing terms of gauge coupling strength such as $\frac{1}{2}g_1 \tilde{B} \nu \nu_L$ and $g_L \tilde{B}_L \nu \nu_L$, where \tilde{B} and \tilde{B}_L are the hypercharge and lepton number gauginos respectively. The size of R-parity violation is related to the neutrino sector and is therefore small. Phenomenologically, this means that SUSY processes proceed as if R-parity is conserved except for the decay of the LSP, which can now decay into SM states. More specifically, SUSY particles are still pair produced. For specific decay channels for a given LSP, see for example [80].

A further interesting consequence is that a sizable VEV can only be realized for one generation of right-handed sneutrinos. This means that lepton number is broken by one unit only in one generation and it is only the corresponding generation of right-handed neutrinos which attains a TeV scale mass; the other two right-handed, or sterile neutrinos, attain sub-eV masses [81, 82, 83]. This has important consequences for cosmology in the form of dark radiation in the early universe and for neutrino oscillation anomalies.

5.3 Dark Matter Candidates

After symmetry breaking, the lightest leptoquark is stable due to the remnant Z_2 symmetry as discussed earlier. This particle must be neutral and could play the role of dark matter. Furthermore, unlike in R-parity conservation, the lightest leptoquark can be either a fermion or a scalar. The best candidates are the \hat{X} and \hat{X}^c superfields since they do not couple to the Z . In this study we assume the lightest leptoquark is the fermionic component of \hat{X} and \hat{X}^c , whose Dirac spinor we refer to as \tilde{X} , and focus on its properties. It is also interesting to note that because the mass of \tilde{X} is given by the VEV of S_2 , it is automatically at the SUSY scale and therefore WIMP-like. This would not be true if its mass was simply

a parameter in the superpotential whose magnitude would be arbitrary. Of course, there is a trade off here with the μ -type problem associated with the μ_{BL} parameter.

The fermionic dark matter candidate can annihilate into two fermions through the neutral gauge bosons present in the theory:

$$\tilde{X}\tilde{X} \rightarrow Z_i \rightarrow \bar{f}f. \quad (5.30)$$

The relevant interactions in this case are

$$\begin{aligned} -\mathcal{L} &= g_B \tilde{X} \gamma^\mu (-B_2 P_L + B_1 P_R) Z_{B\mu} \tilde{X} \\ &+ g_L \tilde{X} \gamma^\mu (-L_2 P_L + L_1 P_R) Z_{L\mu} \tilde{X}, \end{aligned} \quad (5.31)$$

which in the physical basis reads as

$$\begin{aligned} -\mathcal{L} &= g_B \tilde{X} \gamma^\mu (C_{11} P_L + C_{12} P_R) Z_{1\mu} \tilde{X} \\ &+ g_B \tilde{X} \gamma^\mu (C_{21} P_L + C_{22} P_R) Z_{2\mu} \tilde{X}, \end{aligned} \quad (5.32)$$

where

$$C_{11} = -B_2 \cos \theta_{BL} + \frac{g_L}{g_B} L_2 \sin \theta_{BL}, \quad (5.33)$$

$$C_{12} = B_1 \cos \theta_{BL} - \frac{g_L}{g_B} L_1 \sin \theta_{BL}, \quad (5.34)$$

$$C_{21} = -B_2 \sin \theta_{BL} - \frac{g_L}{g_B} L_2 \cos \theta_{BL}, \quad (5.35)$$

$$C_{22} = B_1 \sin \theta_{BL} + \frac{g_L}{g_B} L_1 \cos \theta_{BL}. \quad (5.36)$$

Assuming the contribution from Z_1 dominates, we find an annihilation cross section

$$\sigma v = \sum_q \frac{g_B^4 \tilde{C}}{36\pi s} \frac{\sqrt{1 - 4m_q^2/s}}{(s - M_{Z_1}^2)^2 + \Gamma_{Z_1}^2 M_{Z_1}^2}, \quad (5.37)$$

where

$$\begin{aligned}\tilde{C} &= [(C_{11}^2 + C_{12}^2)(s + 2m_q^2)(s - M_{\tilde{X}}^2) \\ &+ 6 C_{11}C_{12}M_{\tilde{X}}^2(s + 2m_q^2)] \cos^2 \theta_{BL},\end{aligned}\quad (5.38)$$

This cross section is given by

$$(\sigma v)_{NR} = \sum_q \frac{g_B^4}{24\pi} \frac{\sqrt{1 - m_q^2/M_{\tilde{X}}^2}}{(4M_{\tilde{X}}^2 - M_{Z_1}^2)^2 + \Gamma_{Z_1}^2 M_{Z_1}^2} C^2 (2M_{\tilde{X}}^2 + m_q^2), \quad (5.39)$$

in the non-relativistic limit. Here we have defined

$$C = (C_{11} + C_{12}) \cos \theta_{BL}. \quad (5.40)$$

In the present epoch the energy density of the relic dark matter particles \tilde{X} would be,

$$\Omega_{\tilde{X}} h^2 \simeq \frac{x_f}{\sqrt{g_*} \sigma_0 M_P} \frac{(1.07 \times 10^9)}{\text{GeV}}. \quad (5.41)$$

We adopt the value $\Omega_{DM}^{\text{obs}} h^2 = 0.1199 \pm 0.0027$ [76].

The freeze-out temperature $x_f = M_{\tilde{X}}/T_f$ is then given by,

$$x_f = \ln\left(\frac{0.038 g M_P M_{\tilde{X}} \sigma_0}{\sqrt{g_*}}\right) - \frac{1}{2} \ln\left[\ln\left(\frac{0.038 g M_P M_{\tilde{X}} \sigma_0}{\sqrt{g_*}}\right)\right], \quad (5.42)$$

where g is the number of internal degrees of freedom (in our case $g = 4$), g_* is the effective number of relativistic degrees of freedom evaluated around the freeze-out temperature, M_P is the Planck mass, and we use the expansion $\sigma v = \sigma_0 + \sigma_1 v^2$.

The direct detection also proceeds through the Z_i :

$$\tilde{X} N \rightarrow Z_i \rightarrow \tilde{X} N, \quad (5.43)$$

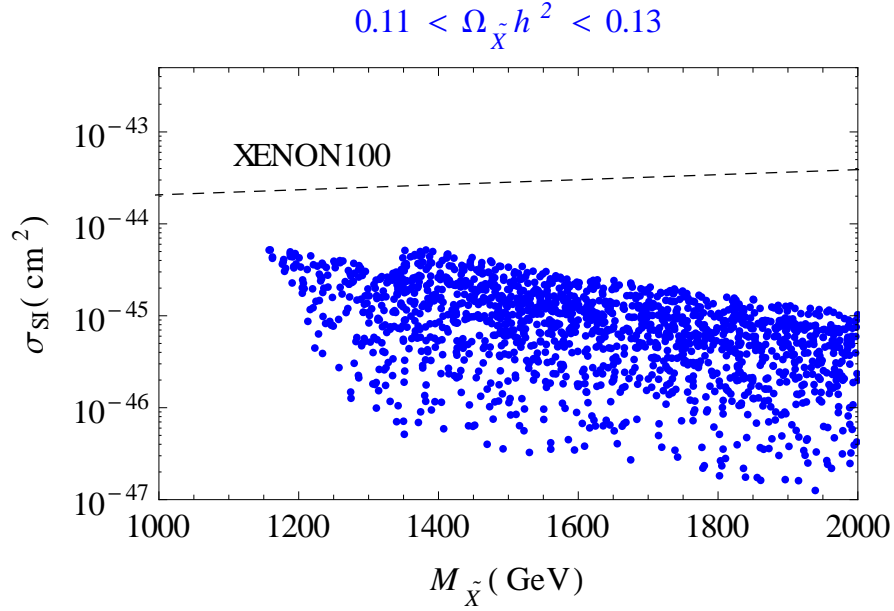


Figure 5.1: Predictions for the elastic nucleon-dark matter cross section for different values of the dark matter mass when $0.11 < \Omega_{\tilde{\chi}} h^2 < 0.13$.

and the spin-independent nucleon-dark matter cross section is then given by

$$\sigma_{\text{SI}} = \frac{1}{4\pi} \frac{M_{\tilde{\chi}}^2 M_N^2}{(M_{\tilde{\chi}} + M_N)^2} \frac{g_B^4}{M_{Z_1}^4} C^2, \quad (5.44)$$

assuming that the dominant contribution comes from the Z_1 gauge boson. Because both the dark matter annihilation and direct detection proceed through Z_1 , they are intimately related to each other. Specifically, once one determines the parameters that yield the correct relic density for a given dark matter mass, there are no free parameters left to hide it from direct detection. Keeping this in mind we present the predictions for the direct detection experiments.

In Fig. 5.1 we show the values for the spin independent cross section versus the dark matter mass when $C = 1$, $0.1 \leq g_B \leq 0.3$, $2.5 \text{ TeV} \leq M_{Z_1} \leq 5 \text{ TeV}$, and assuming that the relic density is in the range $0.11 < \Omega_{\tilde{\chi}} h^2 < 0.13$. One can appreciate in Fig. 5.1 that the allowed solutions are below the XENON100 bounds [84], but could be tested in future dark matter experiments such as XENON1T or LUX.

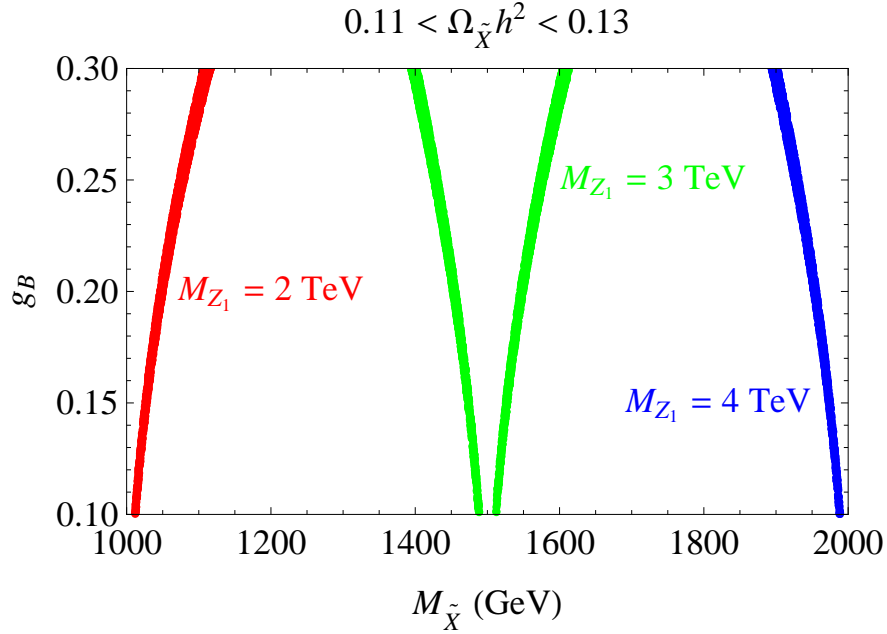


Figure 5.2: Allowed values for the gauge coupling and the dark matter mass when $0.11 < \Omega_{\tilde{\chi}} h^2 < 0.13$ and $M_{Z_1} = 2, 3, 4 \text{ TeV}$.

In Fig. 5.2 we show some solutions when the mass of new lightest neutral gauge boson is 2, 3, or 4 TeV. One can see that there is no need to be very close to the resonance to achieve the required cross section for the relic density.

5.4 Conclusions

In this article we have presented the simplest supersymmetric extension of the model proposed in Ref. [72] where baryon and lepton number are local symmetries. In this context the baryonic and leptonic gauge symmetries are broken at the SUSY scale and the proton is stable.

One of the main predictions of this theory is that R-parity must be spontaneously broken in the MSSM sector because the right-handed sneutrino VEVs are needed to break the remnant local $U(1)_{B-L}$ that results from the VEVs of S_1 and S_2 . Even though R-parity

is broken, the lightest leptoquark is stable and can be a cold dark matter candidate. The dark matter candidate can be either the spin one-half or spin zero SM singlet leptoquark; we have focused on the former in this paper. It furthermore has baryon and lepton number and therefore couples to the two Z 's in the model.

There are many interesting predictions for the Large Hadron Collider searches in this theory. Since R-parity is broken in the MSSM sector we will have lepton number violating signatures at the LHC. For example, one can have exotic channels with four leptons and four jets where three of the leptons have the same electric charge [80, 85]. On the other hand there is a stable dark matter candidate in the theory which can be produced through the new neutral gauge bosons. Therefore, one can also expect signatures with missing energy at the LHC. This theory provides a simple example of very exotic supersymmetric signatures at colliders since one can have the simultaneous presence of R-parity violating and missing energy signatures at the LHC.

Bibliography

- [1] H. Nishino *et al.* [Super-Kamiokande Collaboration], *Search for proton decay via $p \rightarrow e^+\pi^0$ and $p \rightarrow \mu^+\pi^0$ in a Large Water Cherenkov Detector*, Phys. Rev. Lett. **102**, 141801 (2009) [arXiv:0903.0676 [hep-ex]].
- [2] P. Nath and P. Fileviez Perez, *Proton stability in grand unified theories, in strings and in branes*, Phys. Rept. **441**, 191 (2007) [hep-ph/0601023].
- [3] S. M. Barr and X. Calmet, *Observable proton decay from Planck scale physics*, arXiv:1203.5694 [hep-ph].
- [4] J. P. Bowes, R. Foot and R. R. Volkas, *Electric charge quantization from gauge invariance of a Lagrangian: A catalog of baryon number violating scalar interactions*, Phys. Rev. D **54**, 6936 (1996) [hep-ph/9609290].
- [5] I. Baldes, N. F. Bell and R. R. Volkas, *Baryon number violating scalar diquarks at the LHC*, Phys. Rev. D **84**, 115019 (2011) [arXiv:1110.4450 [hep-ph]].
- [6] I. Dorsner, S. Fajfer and N. Kosnik, *Heavy and light scalar leptoquarks in proton decay*, Phys. Rev. D **86**, 015013 (2012) [arXiv:1204.0674 [hep-ph]].
- [7] M. D. Litos, *A search for dinucleon decay into kaons using the SK water cherenkov detector*, Ph. D. Thesis, Boston University, 2012.
- [8] Y. Kamyshev, *Search for matter-antimatter transformation with cold neutrons*, Spontaneous Workshop VI, Cargèse, May 11, 2012.

- [9] R. N. Mohapatra and R. E. Marshak, *Local B-L symmetry of electroweak interactions, Majorana neutrinos and neutron oscillations*, Phys. Rev. Lett. **44**, 1316 (1980) [Erratum-ibid. **44**, 1643 (1980)].
- [10] T. -K. Kuo and S. T. Love, *Neutron oscillations and the existence of massive neutral leptons*, Phys. Rev. Lett. **45**, 93 (1980).
- [11] J. F. Nieves, *Baryon and lepton number nonconserving processes and intermediate mass scales*, Nucl. Phys. B **189**, 182 (1981).
- [12] M. Ozer, *Neutron anti-neutron oscillations and renormalization effects for $\Delta B = 2$ six quark operators*, Phys. Rev. D **26**, 3159 (1982).
- [13] M. I. Buchoff, C. Schroeder and J. Wasem, *Neutron-antineutron oscillations on the lattice*, arXiv:1207.3832 [hep-lat].
- [14] Z. Berezhiani and F. Nesti, *Magnetic anomaly in UCN trapping: signal for neutron oscillations to parallel world?*, Eur. Phys. J. C **72**, 1974 (2012) [arXiv:1203.1035 [hep-ph]].
- [15] K. S. Babu and R. N. Mohapatra, *Coupling unification, GUT-scale baryogenesis and neutron-antineutron oscillation in $SO(10)$* , Phys. Lett. B **715**, 328 (2012) [arXiv:1206.5701 [hep-ph]].
- [16] S. Weinberg, *Varieties of baryon and lepton nonconservation*, Phys. Rev. D **22**, 1694 (1980).
- [17] M. K. Gaillard and B. W. Lee, *Rare decay modes of the K-mesons in gauge theories*, Phys. Rev. D **10**, 897 (1974).
- [18] N. Tsutsui *et al.* [CP-PACS and JLQCD Collaborations], *Lattice QCD calculation of the proton decay matrix element in the continuum limit*, Phys. Rev. D **70**, 111501 (2004) [hep-lat/0402026].

- [19] S. Rao and R. Shrock, $n \leftrightarrow \bar{n}$ transition operators and their matrix elements in the MIT bag model, *Phys. Lett. B* **116**, 238 (1982).
- [20] K. Abe *et al.* [Super-Kamiokande Collaboration], *The search for $n - \bar{n}$ oscillation in Super-Kamiokande I*, arXiv:1109.4227 [hep-ex].
- [21] P. Richardson and D. Winn, *Simulation of sextet diquark production*, *Eur. Phys. J. C* **72**, 1862 (2012) [arXiv:1108.6154 [hep-ph]].
- [22] E. L. Berger, Q. -H. Cao, C. -R. Chen, G. Shaughnessy and H. Zhang, *Color sextet scalars in early LHC experiments*, *Phys. Rev. Lett.* **105**, 181802 (2010) [arXiv:1005.2622 [hep-ph]].
- [23] C. -R. Chen, W. Klemm, V. Rentala and K. Wang, *Color sextet scalars at the CERN Large Hadron Collider*, *Phys. Rev. D* **79**, 054002 (2009) [arXiv:0811.2105 [hep-ph]].
- [24] C. A. Baker, D. D. Doyle, P. Geltenbort, K. Green, M. G. D. van der Grinten, P. G. Harris, P. Iaydjiev and S. N. Ivanov *et al.*, *Improved experimental limit on the electric dipole moment of the neutron*, *Phys. Rev. Lett.* **97**, 131801 (2006) [hep-ex/0602020].
- [25] G. Isidori, Y. Nir and G. Perez, *Flavor physics constraints for physics beyond the standard model*, *Ann. Rev. Nucl. Part. Sci.* **60** (2010) 355 [arXiv:1002.0900 [hep-ph]].
- [26] D. V. Nanopoulos and S. Weinberg, *Mechanisms for cosmological baryon production*, *Phys. Rev. D* **20**, 2484 (1979).
- [27] J. A. Harvey and M. S. Turner, *Cosmological baryon and lepton number in the presence of electroweak fermion number violation*, *Phys. Rev. D* **42**, 3344 (1990).
- [28] K. S. Babu and R. N. Mohapatra, *B-L violating nucleon decay and GUT scale baryogenesis in $SO(10)$* , *Phys. Rev. D* **86**, 035018 (2012) [arXiv:1203.5544 [hep-ph]].

- [29] J. Adam *et al.* [MEG Collaboration], Phys. Rev. Lett. **107**, 171801 (2011).
- [30] R. J. Abrams *et al.* [Mu2e Collaboration], arXiv:1211.7019 [physics.ins-det].
- [31] Y. Kuno *et al.* [COMET Collaboration], Prog. Theor. Exp. Phys. **2013**, 022C01.
- [32] W. Buchmuller, R. Ruckl and D. Wyler, Phys. Lett. B **191**, 442 (1987) [Erratum-ibid. B **448**, 320 (1999)].
- [33] A. J. Davies and X. -G. He, Phys. Rev. D **43**, 225 (1991).
- [34] S. Davidson, D. C. Bailey and B. A. Campbell, Z. Phys. C **61**, 613 (1994).
- [35] E. Gabrielli, Phys. Rev. D **62**, 055009 (2000).
- [36] R. Benbrik and C. -K. Chua, Phys. Rev. D **78**, 075025 (2008).
- [37] I. Dorsner, S. Fajfer, J. F. Kamenik and N. Kosnik, Phys. Lett. B **682**, 67 (2009).
- [38] R. Benbrik, M. Chabab and G. Faisel, arXiv:1009.3886 [hep-ph].
- [39] M. Gonderinger and M. J. Ramsey-Musolf, JHEP **1011**, 045 (2010) [Erratum-ibid. **1205**, 047 (2012)].
- [40] J. M. Arnold, B. Fornal and M. B. Wise, Phys. Rev. D **87**, 075004 (2013).
- [41] R. Kitano, M. Koike and Y. Okada, Phys. Rev. D **66**, 096002 (2002) [Erratum-ibid. D **76**, 059902 (2007)].
- [42] V. Cirigliano, R. Kitano, Y. Okada and P. Tuzon, Phys. Rev. D **80**, 013002 (2009).
- [43] P. Wintz, [for the SINDRUM Collaboration] Conf. Proc. C **980420**, 534 (1998).
- [44] T. Suzuki, D. F. Measday and J. P. Roalsvig, Phys. Rev. C **35**, 2212 (1987).
- [45] J. J. Hudson, D. M. Kara, I. J. Smallman, B. E. Sauer, M. R. Tarbutt and E. A. Hinds, Nature **473**, 493 (2011).

- [46] H. Nishino *et al.* [Super-Kamiokande Collaboration], Phys. Rev. Lett. **102**, 141801 (2009).
- [47] M. Drees and G. Gerbier, “Mini-Review of Dark Matter: 2012,” in [Particle Data Group Collaboration], Phys. Rev. D **86** (2012) 010001.
- [48] H. Goldberg, “Constraint on the Photino Mass from Cosmology,” Phys. Rev. Lett. **50** (1983) 1419 [Erratum-ibid. **103** (2009) 099905].
- [49] J. R. Ellis, J. S. Hagelin, D. V. Nanopoulos, K. A. Olive and M. Srednicki, “Supersymmetric Relics from the Big Bang,” Nucl. Phys. B **238** (1984) 453.
- [50] G. Jungman, M. Kamionkowski and K. Griest, “Supersymmetric dark matter,” Phys. Rept. **267** (1996) 195 [hep-ph/9506380].
- [51] W. Buchmuller, “Gravitino Dark Matter,” AIP Conf. Proc. **1200** (2010) 155 [arXiv:0910.1870 [hep-ph]].
- [52] L. M. Krauss and F. Wilczek, “Discrete Gauge Symmetry in Continuum Theories,” Phys. Rev. Lett. **62** (1989) 1221.
- [53] S. P. Martin, “Some simple criteria for gauged R-parity,” Phys. Rev. D **46** (1992) 2769 [hep-ph/9207218].
- [54] C. S. Aulakh, A. Melfo, A. Rasin and G. Senjanovic, “Seesaw and supersymmetry or exact R-parity,” Phys. Lett. B **459** (1999) 557 [hep-ph/9902409].
- [55] C. S. Aulakh, B. Bajc, A. Melfo, A. Rasin and G. Senjanovic, “SO(10) theory of R-parity and neutrino mass,” Nucl. Phys. B **597** (2001) 89 [hep-ph/0004031].
- [56] K. S. Babu and R. N. Mohapatra, “Minimal Supersymmetric Left-Right Model,” Phys. Lett. B **668** (2008) 404 [arXiv:0807.0481 [hep-ph]].

- [57] D. Feldman, P. Fileviez Perez and P. Nath, “R-parity Conservation via the Stueckelberg Mechanism: LHC and Dark Matter Signals,” JHEP **1201** (2012) 038 [arXiv:1109.2901 [hep-ph]].
- [58] P. Fileviez Perez, S. Spinner and M. K. Trenkel, “Testing the Mechanism for the LSP Stability at the LHC,” Phys. Lett. B **702** (2011) 260 [arXiv:1103.3824 [hep-ph]].
- [59] L. Basso, B. O’Leary, W. Porod and F. Staub, “Dark matter scenarios in the minimal SUSY B-L model,” arXiv:1207.0507 [hep-ph].
- [60] B. O’Leary, W. Porod and F. Staub, “Mass spectrum of the minimal SUSY B-L model,” JHEP **1205** (2012) 042 [arXiv:1112.4600 [hep-ph]].
- [61] P. Fileviez Perez, S. Spinner and M. K. Trenkel, “The LSP Stability and New Higgs Signals at the LHC,” Phys. Rev. D **84** (2011) 095028 [arXiv:1103.5504 [hep-ph]].
- [62] V. Barger, P. Fileviez Perez and S. Spinner, “Minimal gauged U(1)(B-L) model with spontaneous R-parity violation,” Phys. Rev. Lett. **102** (2009) 181802 [arXiv:0812.3661 [hep-ph]].
- [63] P. Fileviez Perez and S. Spinner, “The Minimal Theory for R-parity Violation at the LHC,” JHEP **1204** (2012) 118 [arXiv:1201.5923 [hep-ph]].
- [64] O. Lahav and A. R. Liddle, “The Cosmological Parameters,”
<http://pdg.lbl.gov/2012/reviews/rpp2012-rev-cosmological-parameters.pdf>
- [65] E. Aprile *et al.* [XENON100 Collaboration], “Dark Matter Results from 100 Live Days of XENON100 Data,” Phys. Rev. Lett. **107**, 131302 (2011) [arXiv:1104.2549 [astro-ph.CO]].
- [66] J. Angle *et al.* [XENON10 Collaboration], “A search for light dark matter in XENON10 data,” Phys. Rev. Lett. **107** (2011) 051301 [arXiv:1104.3088 [astro-ph.CO]].

- [67] V. Barger, P. Fileviez Perez and S. Spinner, *Minimal gauged $U(1)_{B-L}$ model with spontaneous R -parity violation*, Phys. Rev. Lett. **102** (2009) 181802 [arXiv:0812.3661 [hep-ph]].
- [68] C. S. Aulakh, A. Melfo, A. Rasin and G. Senjanovic, *Seesaw and supersymmetry or exact R -parity*, Phys. Lett. B **459**, 557 (1999) [hep-ph/9902409].
- [69] C. S. Aulakh, B. Bajc, A. Melfo, A. Rasin and G. Senjanovic, *$SO(10)$ theory of R -parity and neutrino mass*, Nucl. Phys. B **597**, 89 (2001) [hep-ph/0004031].
- [70] K. S. Babu and R. N. Mohapatra, *Minimal Supersymmetric Left-Right Model*, Phys. Lett. B **668**, 404 (2008) [arXiv:0807.0481 [hep-ph]].
- [71] P. Nath and P. Fileviez Perez, *Proton stability in grand unified theories, in strings and in branes*, Phys. Rept. **441**, 191 (2007) [hep-ph/0601023].
- [72] M. Duerr, P. Fileviez Perez and M. B. Wise, *Gauge theory for baryon and lepton numbers with leptoquarks*, Phys. Rev. Lett. **110**, 231801 (2013) [arXiv:1304.0576 [hep-ph]].
- [73] P. Fileviez Perez and M. B. Wise, *Baryon and lepton number as local gauge symmetries*, Phys. Rev. D **82**, 011901 (2010) [Erratum-ibid. D **82**, 079901 (2010)] [arXiv:1002.1754 [hep-ph]].
- [74] P. Fileviez Perez and M. B. Wise, *Breaking local baryon and lepton number at the TeV scale*, JHEP **1108**, 068 (2011) [arXiv:1106.0343 [hep-ph]].
- [75] M. Duerr and P. Fileviez Perez, *Baryonic Dark Matter*, arXiv:1309.3970 [hep-ph].
- [76] P. A. R. Ade *et al.* [Planck Collaboration], *Planck 2013 results. XVI. Cosmological parameters*, arXiv:1303.5076 [astro-ph.CO].
- [77] H. An, R. Huo and L. -T. Wang, *Searching for Low Mass Dark Portal at the LHC*, Phys. Dark Univ. **2**, 50 (2013) [arXiv:1212.2221 [hep-ph]].

- [78] B. A. Dobrescu and F. Yu, *Coupling–mass mapping of di-jet peak searches*, Phys. Rev. D **88**, 035021 (2013) [arXiv:1306.2629 [hep-ph]].
- [79] M. S. Carena, A. Daleo, B. A. Dobrescu and T. M. P. Tait, *Z' gauge bosons at the Tevatron*, Phys. Rev. D **70**, 093009 (2004) [hep-ph/0408098].
- [80] P. Fileviez Perez and S. Spinner, *The Minimal Theory for R-parity Violation at the LHC*, JHEP **1204**, 118 (2012) [arXiv:1201.5923 [hep-ph]].
- [81] R. N. Mohapatra, *Mechanism for Understanding Small Neutrino Mass in Superstring Theories*, Phys. Rev. Lett. **56**, 561 (1986).
- [82] D. K. Ghosh, G. Senjanovic and Y. Zhang, *Naturally Light Sterile Neutrinos from Theory of R-parity*, Phys. Lett. B **698**, 420 (2011) [arXiv:1010.3968 [hep-ph]].
- [83] V. Barger, P. Fileviez Perez and S. Spinner, *Three Layers of Neutrinos*, Phys. Lett. B **696**, 509 (2011) [arXiv:1010.4023 [hep-ph]].
- [84] E. Aprile *et al.* [XENON100 Collaboration], *Dark Matter Results from 225 Live Days of XENON100 Data*, Phys. Rev. Lett. **109**, 181301 (2012) [arXiv:1207.5988 [astro-ph.CO]].
- [85] P. Fileviez Perez and S. Spinner, *Supersymmetry at the LHC and The Theory of R-parity*, arXiv:1308.0524 [hep-ph].